Thesis Proposal:
Nanostructures with Topological Insulators

Mahmoud Lababidi

December 13, 2011

Contents

1 Introduction **2**
- 1.1 Overview . . . 2
- 1.2 Motivation and Background . . . 2

2 Metal to Topological Insulator Scattering **4**
- 2.1 Introduction . . . 4
- 2.2 Model Hamiltonian and Complex Band Structure . . . 5
- 2.3 Scattering Matrix from Wave-Function Matching . . . 7
- 2.4 Interface Spectrum and Scattering Matrix from Lattice Green Function . . . 9
- 2.5 Discussions . . . 11

3 Superconducting Proximity Effect **12**
- 3.1 Introduction . . . 12
- 3.2 Model and Basic Equations . . . 14
- 3.3 Fourier Expansion . . . 17
- 3.4 The Order Parameter . . . 18
- 3.5 The Interface Mode and the Fu-Kane Model . . . 20
- 3.6 Triplet Pair Correlations . . . 22
- 3.7 Summary . . . 25

4 Josephson Junction on TI Surface **26**
- 4.1 Introduction . . . 26
- 4.2 Model and Basic Equations . . . 26
- 4.3 Energy Spectrum . . . 29
- 4.4 Order Parameter and Singlet Correlation . . . 30
- 4.5 Local Density of States . . . 31
- 4.6 Spectral Function . . . 33
- 4.7 Summary . . . 33

5 TI-FET: MOSFET with a Topological Insulator **34**
- 5.1 Introduction . . . 34
- 5.2 MOSFET . . . 35
- 5.3 TI as the Floating Gate . . . 36
- 5.4 TI as the Current Channel . . . 37
- 5.5 Summary . . . 37

Chapter 1

Introduction

1.1 Overview

In this proposal I will have four parts that break down the why, how and what I propose to do in my research for my thesis. I begin by presenting a brief introduction to topological insulators (TIs) which can be skipped for brevity if one is already familiar with the subject. This introduction will not be as detailed as many papers on the subject but should suffice for understanding the proposed actions in this proposal. Then I will highlight some novel and interesting physics that have been spurred by the discovery of TIs. This is simply to motivate the projects that I have and will work on. Next, I will present work already completed and in progress. Lastly, I will present future projects that I aim to complete towards my research.

1.2 Motivation and Background

Topological Insulators (TIs) are new forms of matter that have robust conducting metallic surface states while the bulk is an insulator. The surface is so vastly different from the bulk, that it can be seen as a playground of new properties never seen before. One such novel property is that the surface is host to Dirac Fermions which behave relativistically with zer mass. These particles are identified as Dirac Fermions because they obey the Dirac equation which models relativistic (near speed of light) particles. These massless relativistic Fermions, demonstrate a direct linear relationship between the energy (E) and their quantized momentum (k), $E = \pm\hbar v k$. This peculiar energy relationship is uncommon in materials.

This low energy linear dispersion is described by the Hamiltonian

$$H = \vec{\sigma} \cdot \vec{k} - \mu = \sigma_x k_x + \sigma_y k_y - \mu. \tag{1.1}$$

On the surface, the spin and momentum direction of the electron are locked. This locking is due to the spin-orbit coupling that is similarly found in Rashba spin-orbit coupled materials [1].

The insulator component exists due to the fact that the SOC actually causes the bulk of the material to have a fully gapped energy spectrum while the robust surface Hamiltonian is a result of the surface boundary. This robustness is also a result of the non-trivial topological nature of the material. These surface states are not an accident due to possible band crossing but rather a definition of a topological phase transition from the bulk to the boundary.

TIs have attracted much attention for a variety of new physics. Such physics include the proposal to generate Majorana particles, which are non-Abelian, through the use of superconductors in proximity; interesting conductance on the surface due to the Dirac-like Hamiltonian and spin

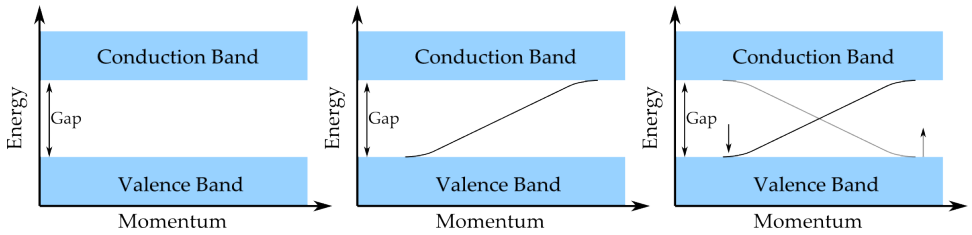

Figure 1.1: (a) Energy spectrum of a trivial band insulator (b) Energy spectrum of a quantum hall state, where one crossing line extends from the valence band to the conduction band. (c) Energy spectrum of a topological insulator. The gapped bands are the bulk conduction and valence bands while the extended lines represent quantum hall like states. One line is for the spin up states and the other is for the spin down states. This essentially mimics two copies of the quantum hall state for each spin state.

(eg Klein Tunneling); and the possibility of new topological phases of materials. Already many predictions for topological superconductors have been made and realizations of such materials have hit the scene. The Majorana particles have been proposed to be used in topological quantum computation.

TIs can also be used in possible electronic spintronic applications. Such spintronic devices based on TIs will almost inevitably involve metal as measurement probes or functioning components [2]. This motivates us to study the local spectrum near the interface between a metal (M) and a topological insulator (TI). For a metal-ordinary semiconductor junction with good contact, it is well known that the metallic Bloch states penetrate into the semiconductor as evanescent waves localized at the interface (for energies within the band gap). Such interface states are known as metal induced gap states (MIGS) [3, 4]. They play an important role in controlling the junction properties, e.g., by pinning the semiconductor Fermi level to determine the Schottky barrier height [5], a key parameter of the junction.

Chapter 2

Metal to Topological Insulator Scattering

We compute the spin-active scattering matrix and the local spectrum at the interface between a metal and a three-dimensional topological band insulator. We show that there exists a critical incident angle at which complete (100%) spin flip reflection occurs and the spin rotation angle jumps by π. We discuss the origin of this phenomena, and systematically study the dependence of spin-flip and spin-conserving scattering amplitudes on the interface transparency and metal Fermi surface parameters. The interface spectrum contains a well-defined Dirac cone in the tunneling limit, and smoothly evolves into a continuum of metal induced gap states for good contacts. We also investigate the complex band structure of Bi_2Se_3.

2.1 Introduction

Recently discovered three dimensional topological band insulators [6, 7, 8], such as $Bi_{1-x}Sb_x$ [9] and Bi_2Se_3 [10, 11, 12], are spin-orbit coupled crystal solids with a bulk gap but protected gapless surface states. The low energy excitations at the surface are helical Dirac fermions, i.e., their spin and momentum are entangled (locked) [13]. The charge and spin transport on the surface of a topological insulator are intrinsically coupled [14]. This makes these materials a promising new platform for spintronics. In addition, heterostructures involving topological insulator, superconductor, and/or ferromagnet have been predicted to show a remarkable array of novel spectral and transport properties (for review see Ref. [15, 16, 17]).

Electronic or spintronic devices based on topological insulators will almost inevitably involve metal as measurement probes or functioning components [2]. This motivates us to study the local spectrum near the interface between a metal (M) and a topological insulator (TI). For a metal-ordinary semiconductor junction with good contact, it is well known that the metallic Bloch states penetrate into the semiconductor as evanescent waves localized at the interface (for energies within the band gap). Such interface states are known as metal induced gap states (MIGS) [3, 4]. They play an important role in controlling the junction properties, e.g., by pinning the semiconductor Fermi level to determine the Schottky barrier height [5], a key parameter of the junction.

The local spectrum at the M-TI junction is intimately related to the spin-active scattering of electrons at the M-TI interface. In this paper, we systematically study the evolution of the scattering matrix and the interface spectra with the junction transparency and metal Fermi surface parameters. The scattering matrix [18] we obtain here also forms the basis to investigate the details of the superconducting proximity effect near the superconductor-TI interface [19], which was shown

by Fu and Kane to host Majorana fermions [20].

The scattering at the M-TI interface differs significantly from its two dimensional analog, the interface between a metal and a quantum spin Hall (QSH) insulator studied by Tokoyama et al [2]. They predicted a giant spin rotation angle $\alpha \sim \pi$ and interpreted the enhancement as resonance with the one-dimensional helical edge modes. By contrast, for M-TI interface we predict a critical incident angle at which complete spin flipping occurs and the spin rotation angle jumps by π. We will explain its origin, in particular its relation to the surface helical Dirac spectrum, and discuss its spintronic implications.

This paper is organized as follows. We will first compute the scattering matrix using a $\mathbf{k}\cdot\mathbf{p}$ continuum model by matching the envelope wave functions at the M-TI interface. This simple calculation is easy to understand, and it brings out the main physics of our problem. Along the way, we will discuss the complex band structure of Bi_2Se_3, which describes the decaying (rather than propagating Bloch wave) solutions of the crystal Hamiltonian. The various caveats of this calculation are then remedied by considering a much more general lattice model. Most importantly, it enables us to track how the scattering matrix and interface spectrum change with interface transparency. It also sheds light on the origin of perfect spin-flip scattering at the critical angle. We will show that the results obtained from these two complementary methods are consistent with each.

2.2 Model Hamiltonian and Complex Band Structure

We consider Bi_2Se_3 as a prime example of 3D strong topological insulators. Its low energy $\mathbf{k}\cdot\mathbf{p}$ Hamiltonian was obtained by Zhang et al [11],

$$\hat{H}_{TI}(\mathbf{k}) = \epsilon_0(\mathbf{k})\hat{1} + \sum_{\mu=0}^{3} d_\mu(\mathbf{k})\hat{\Gamma}_\mu.$$

Here $d_0(\mathbf{k}) = M - B_1k_z^2 - B_2(k_x^2+k_y^2)$, $d_1(\mathbf{k}) = A_2k_x$, $d_2(\mathbf{k}) = A_2k_y$, $d_3(\mathbf{k}) = A_1k_z$, and $\epsilon_0(\mathbf{k}) = C + D_1k_z^2 + D_2(k_x^2+k_y^2)$. The numerical values of M, A, B, C, D are given in Ref. [11]. We choose the basis ($|+\uparrow\rangle$, $|+\downarrow\rangle$, $|-\uparrow\rangle$,$|-\downarrow\rangle$), where $\pm$ labels the hybridized p_z orbital with even (odd) parity [11]. The Gamma matrices are defined as $\hat{\Gamma}_0 = \hat{\tau}_3\otimes\hat{1}$, $\hat{\Gamma}_i = \hat{\tau}_1\otimes\hat{\sigma}_i$, with $\hat{\tau}_i$ ($\hat{\sigma}_i$) being the Pauli matrices in the orbital (spin) space. The chemical potential of as-grown Bi_2Se_3 crystal actually lies in the conduction band [13]. By hole doping [13] or applying a gate voltage [21], the chemical potential can be tuned inside the gap. The system is well described by H_{TI} (note that energy zero is set as in the middle of the band gap).

In this section, we first adopt a rather artificial model for metals with negligible spin-orbit coupling. It is obtained by turning off the spin-orbit interaction (setting $d_\mu = 0$ for μ=1,2,3) in H_{TI} and shifting the Fermi level into the conduction band. The result is spin-degenerate two-band Hamiltonian

$$\hat{H}_M(\mathbf{k}) = [\epsilon_0(\mathbf{k}) - E_F]\hat{1} + d_0(\mathbf{k})\hat{\Gamma}_0.$$

Its band structure, schematically shown in Fig. 1(b), consists of two oppositely dispersing bands (the solid and dash line). E_F is tuned to be much higher than the band crossing point, so the scattering properties of low energy electrons near the Fermi surface are insensitive to the band crossing at high energies. This claim will be verified later using a more generic model for the metal. A similar model was used in the study of metal-QSH interface [2].

Matching the wave functions of two dissimilar materials (such as Au and Bi_2Se_3) at interface is in general complicated within the $\mathbf{k}\cdot\mathbf{p}$ formalism, because the envelope wave functions on either

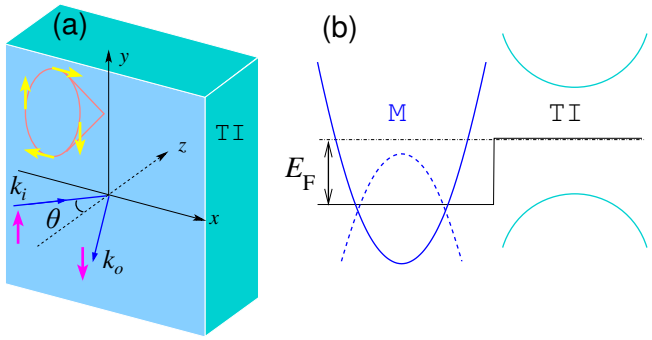

Figure 2.1: (a) Scattering geometry at a metal (M)-topological insulator (TI) interface. (b) Schematic band structure of the metal (modeled by $\hat{H}_M$) and topological insulator.

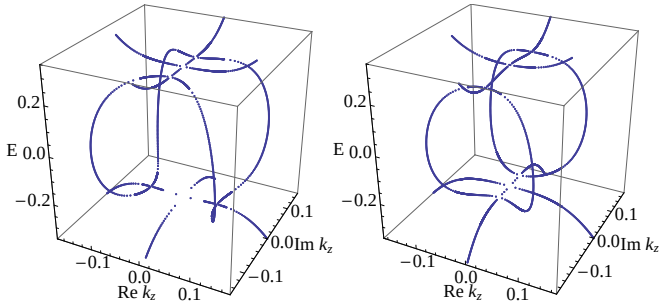

Figure 2.2: The complex band structure of topological insulator described by $\hat{H}_{TI}(\mathbf{k})$ for $k_y = 0$, $k_x = 0.02$ (left) and 0.04 (right). E is measured in eV, and k in $\mathring{A}^{-1}$. Subgap states with complex k_z represent evanescent waves. The topology of real lines [26] changes as k_x is increased.

side are defined using different basis (see Ref. [22] and reference therein). For the particular model H_M, however, such complication is circumvented. Then, then wave functions at the metal-TI interface ($z = 0$) satisfy the Ben-Daniel and Duke boundary condition [23],

$$\hat{\Phi}_M = \hat{\Phi}_{TI}, \quad \hat{v}_M \hat{\Phi}_M = \hat{v}_{TI} \hat{\Phi}_{TI}.$$

Here $\hat{\Phi}_i$ is the four-component wave function, and the velocity matrix $\hat{v}_i = \partial \hat{H}_i / \partial k_z$, $i \in \{M, TI\}$. Such boundary condition assumes good atomic contact between two materials.

We are interested in energies below the band gap of TI, so $\hat{\Phi}_{TI}$ is evanescent in nature and only penetrates into TI for a finite length. Such localized (surface or interface) states inside topological insulator can be treated within the $\mathbf{k} \cdot \mathbf{p}$ formalism using the theory of *complex band structures*, pioneered by Kohn [24], Blount [25], and Heine [26] et al. The main idea is to allow the crystal momentum to be complex and analytically continue $H_{TI}(\mathbf{k})$ to the complex $\mathbf{k}$ plane. While the extended Bloch waves are the eigen states of $H_{TI}(\mathbf{k})$ for real $\mathbf{k}$, eigen functions of $H_{TI}(\mathbf{k})$ for complex $\mathbf{k}$ describe localized states. Together they form a complete basis to describe crystals of finite dimension.

In our scattering problem, we have to find all eigen states of $H_{TI}(\mathbf{k})$ with energy E and wave vector $\mathbf{k} = (k_x, k_y, \tilde{k}_z)$, where k_x and k_y are given and real, but $\tilde{k}_z$ is complex and unknown. For a general $\mathbf{k} \cdot \mathbf{p}$ Hamiltonian such as $\hat{H}_{TI}$, we follow Chang and Schulman [27] to rewrite it as

$$\hat{H}_{TI} = \hat{h}_0(k_x, k_y) + \hat{h}_1 \tilde{k}_z + \hat{h}_2 \tilde{k}_z^2,$$

where $\hat{h}_1 = A_1\hat{\Gamma}_3$, and $\hat{h}_2 = -B_1\hat{\Gamma}_0$. Then the eigen equation $(\hat{H}_{TI} - E\hat{1})\hat{\phi} = 0$ can be reorganized into an eigen value problem for $\tilde{k}_z$,

$$\begin{pmatrix} 0 & 1 \\ -\hat{h}_2^{-1}(\hat{h}_0 - E\hat{1}) & -\hat{h}_2^{-1}\hat{h}_1 \end{pmatrix} \begin{pmatrix} \hat{\phi} \\ \hat{\phi}' \end{pmatrix} = \tilde{k}_z \begin{pmatrix} \hat{\phi} \\ \hat{\phi}' \end{pmatrix}.$$

Then all possible values of $\tilde{k}_z$ can be obtained for given incident parameter E, k_x, and k_y. For the anisotropic Dirac Hamiltonian $H_{TI}(\mathbf{k})$, the energy eigenvalues can be obtained analytically [28], which allows for an analytical solution of the complex band structure.

For E within the gap, there are in general 4 pairs of complex solution of $\tilde{k}_z$, for if $\tilde{k}_z$ is a solution so is $\tilde{k}_z^*$. We label those with positive imaginary parts with $\{\tilde{k}_z^\nu\}$, and the corresponding wave function $\{\hat{\phi}^\nu\}$, $\nu = 1, 2, 3, 4$. They are decaying solutions in the half space $z > 0$. In our model, $\tilde{k}_z$ turns out to be doubly degenerate, as shown in Fig. 2. The wave function inside TI ($z > 0$) then has the form

$$\hat{\Phi}_{TI} = \sum_\nu t_\nu e^{i\tilde{k}_z^\nu z}\hat{\phi}_\nu.$$

2.3 Scattering Matrix from Wave-Function Matching

To set the stage for discussing scattering off a topological insulator, it is instructive to recall the generic features of elastic scattering of electrons by a heavy ion with spin-orbit interaction. This classical problem was solved by Mott, and known as *Mott scattering*. The scattering matrix has the general form [29]

$$\hat{S}_{Mott} = u\hat{1} + w\hat{\boldsymbol{\sigma}} \cdot (\mathbf{k}_i \times \mathbf{k}_o),$$

where $\mathbf{k}_i$ and $\mathbf{k}_o$ are the incident and outgoing momentum respectively, $\hat{\boldsymbol{\sigma}}$ is the Pauli matrix, and u, w depend on the scattering angle. It is customary to define the spin-flip amplitude $f = S_{21}$, and spin-conserving amplitude $g = S_{11}$. Both f and g are complex numbers, their relative phase defines the *spin rotation angle* $\alpha = \mathrm{Arg}(g^* f)$. One immediately sees that for back scattering, $\hat{S}_{Mott} = u\hat{1}$, so there is no spin flip, $f = 0$. As we will show below, this also holds true for scattering off TI.

Now consider an electron coming from the metal with momentum $\mathbf{k}$ incident on the M-TI interface located at $z = 0$, as schematically shown in Fig. 1(a). We assume the interface is translationally invariant, so the transverse momentum $\mathbf{k}_\parallel = (k_x, k_y)$ is conserved, and the energy E of the electron lies within the band gap of TI. Then, only total reflection is possible, but the spin-orbit coupling inside TI acting like a $\mathbf{k}$-dependent magnetic field rotates the spin of the incident particle. The scattering (reflection) matrix has the form

$$\hat{S}(\mathbf{k}) = \begin{pmatrix} g & \bar{f} \\ f & \bar{g} \end{pmatrix},$$

where $|g|^2 + |f|^2 = 1$. Our goal is to find the dependence of the scattering amplitudes f, g on $\mathbf{k}$, or equivalently, on energy E and incident angle θ. From time-reversal symmetry, $\bar{f}(E, \theta) = f(E, -\theta)$ and $\bar{g}(E, \theta) = g(E, -\theta)$. We shall show that $f(\mathbf{k}_\parallel) = -f(-\mathbf{k}_\parallel)$, $g(\mathbf{k}_\parallel) = g(-\mathbf{k}_\parallel)$. So f is an odd function of θ, while g is even in θ. Since our problem can be viewed as coherent multiple scattering from a lattice array of Mott scatters occupying half the space, we will refer to spin-active scattering at the metal-TI interface as Mott scattering.

Consider a spin up electron from the conduction band of the metal with momentum $\mathbf{k}$ and energy $E = \epsilon_0(\mathbf{k}) - E_F - d_0(\mathbf{k})$ lying within the band gap of TI. The wave function inside the metal ($z < 0$) has the form

$$\hat{\Phi}_M = (r_1 e^{-ik_z' z}, r_2 e^{-ik_z' z}, e^{ik_z z} + r_3 e^{-ik_z z}, r_4 e^{-ik_z z})^{\mathrm{T}},$$

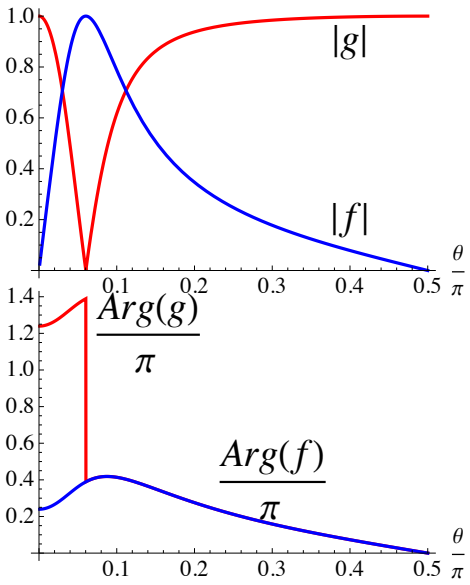

Figure 2.3: The magnitudes (upper panel) and the phases (lower panel) of the spin-flip amplitude f and spin-conserving amplitude g versus the incident angle θ. $E = 0.1$eV, E_F=0.28eV. $|g|^2+|f|^2 = 1$. Arg(g) and Arg(f) are shifted upward by π for clarity.

up to the trivial $e^{i(k_x x+k_y y)}$ and renormalization factor. Here $k_z = \hat{z}\cdot\mathbf{k}$, and $\{r_i\}$ are the reflection amplitudes. We identify the spin flip amplitude $f = r_4$ and the spin-conserving amplitude $g = r_3$. Note that there is no propagating mode at energy E available in the valence band for the reflected electron. So k_z' is purely imaginary. At such energy, there is no propagating mode available in TI. We have discussed the evanescent wave function $\hat{\Phi}_{TI}$ in the previous section. With $\hat{\Phi}_M$ and $\hat{\Phi}_{TI}$, we solve the boundary condition at $z = 0$ to obtain r_ν, t_ν and the scattering matrix S.

Fig. 3 shows the magnitude and phase of f and g versus the incident angle θ for $E = 0.1$eV, with E_F set to be 0.28eV. At normal incidence, $\theta = 0$, spin flip scattering is forbidden as in the single-ion Mott scattering. With increasing θ the magnitude of g drops continuously. At a critical angle θ_c, $|g|$ drops to zero and we have perfect (100%) spin flip reflection. At the same time, the spin rotation angle α (the relative phase between f and g) jumps by π.

It is tantalizing to think of what happens at θ_c as resonant scattering with the helical surface mode of the TI. This however is problematic. We are considering good contacts at which the wave functions of the two materials hybridize strongly. Surface mode is preempted by MIGS. Indeed, we checked that the corresponding critical transverse momentum $k_\parallel$ depends only weakly on E. This is at odds with the linear dispersion of the TI surface mode, $E = A_2 k_\parallel$ [11]. To gain better understanding, we now switch to a lattice model to systematically study the role of interface transparency and metal Fermi surface parameter (E_f, k_f, v_f) on the scattering matrix.

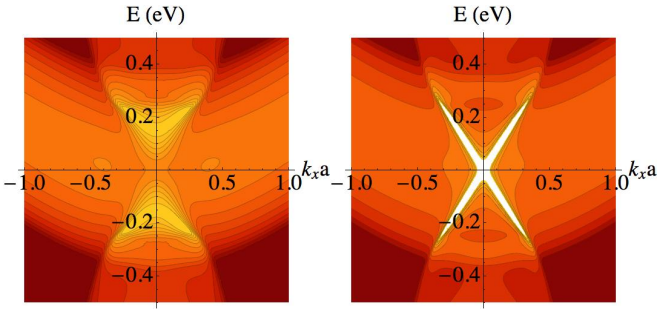

Figure 2.4: The spectral function $N(E, k_x, k_y = 0)$ at the interface of metal and topological insulator. Left: good contact, $J = t_M$, showing the continuum of metal induced gap states. Right: poor contact with low transparency, $J = 0.2t_M$, showing well defined Dirac spectrum as on the TI surface. $t_M = 0.18eV$, $\mu_M = -4t_M$, a is lattice spacing.

2.4 Interface Spectrum and Scattering Matrix from Lattice Green Function

We consider a simple lattice model for the M-TI junction. The topological insulator is modeled by a tight binding Hamiltonian on cubic lattice,

$$\mathscr{H}_R = \sum_{k_+,n} \Big\{ \hat{\psi}^\dagger_{k_+,n}(b_1\hat{\Gamma}_0 - i\tfrac{a_1}{2}\hat{\Gamma}_3)\hat{\psi}_{k_+,n+1} + h.c. \\ + \hat{\psi}^\dagger_{k_+,n}\left[d(k_+)\hat{\Gamma}_0 + a_2(\hat{\Gamma}_1 \sin k_x + \hat{\Gamma}_2 \sin k_y)\right]\hat{\psi}_{k_+,n}\Big\}.$$

Here $\hat{\psi} = (\psi_{+\uparrow}, \psi_{+\downarrow}, \psi_{-\uparrow}, \psi_{-\downarrow})^{\mathrm{T}}$ is the annihilation operator, $d(k_+) = M - 2b_1 + 2b_2(\cos k_x + \cos k_y - 2)$ with k measured in $1/a$. The cubic lattice consists of layers of square lattice stacked in the z direction, n is the layer index, and k_+ is the momentum in the xy plane. The isotropic version of $\mathscr{H}_R$, with $a_1 = a_2$, $b_1 = b_2$, was studied by Qi et al as a minimal model for 3D topological insulators [28]. To mimic Bi_2Se_3, we set the lattice spacing $a = 5.2$Å, which gives the correct unit cell volume, and $a_i = A_i/a$, $b_i = B_i/a^2$ for $i = 1, 2$. Although a crude caricature of the real material, $\mathscr{H}_R$ yields the correct gap size and surface dispersion, it also reduces to the continuum $\mathbf{k}\cdot\mathbf{p}$ Hamiltonian $\hat{H}_{TI}$ in the small k limit, aside from the topologically trivial $\epsilon_0(\mathbf{k})$ term.

As a generic model for metal, we consider a single band tight binding Hamiltonian on cubic lattice,

$$\mathscr{H}_L = \sum_{k_+,n,\sigma} [h(k_+)n_{k_+,n,\sigma} - t_M\phi^\dagger_{k_+,n,\sigma}\phi_{k_+,n+1,\sigma} + h.c.]$$

where $h(k_+) = -2t_M(\cos k_x + \cos k_y) - \mu_M$. The Fermi surface parameters of the metal can be varied by tuning t_M and μ_M. The metal occupies the left half space, $n \le 0$, and the TI occupies the right half space $n \ge 1$. The interface domain consists of layer $n = 0, 1$. The coupling between metal and TI is described by hopping,

$$\mathscr{H}_{LR} = -\sum_{k_+,\ell,\sigma} J_\ell \psi^\dagger_{k_+,n=1,\ell,\sigma}\phi_{k_+,n=0,\sigma} + h.c.$$

J_ℓ is the overlap integral between the p-orbital $\ell = \pm$ of TI and the s-like orbital of metal. For simplicity, we assume J_ℓ is independent of spin. Then, $J_+ = -J_- = J$. J can be tuned from weak to strong. Small J mimics a large tunneling barrier between M and TI, and large J (comparable to t_M or B_2) describes a good contact.

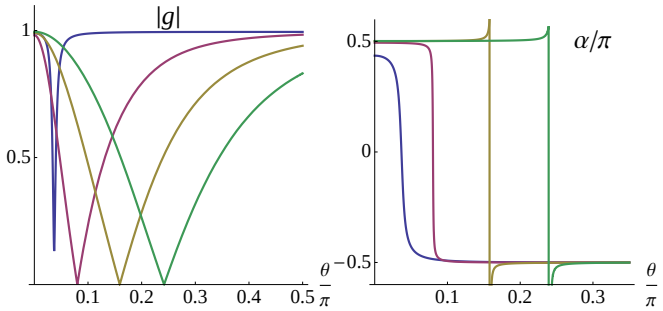

Figure 2.5: The spin-conserving reflection amplitude $|g|$ and spin rotation angle α versus the incident angle θ for increasing contact transparency, $J/t_M = 0.25, 1, 1.5, 2$ (from left to right). $t_M = 0.18eV$, $\mu_M = -4t_M$, $E = 0.05$eV, $k_y = 0$. $|f|^2 = 1 - |g|^2$.

The lattice Green function of the composite system is computed via standard procedure by introducing the inter-layer transfer matrix and the method of interface Green function matching [30]. Fig. 4 shows two examples of the local spectral function (momentum-resolved density of states) at the interface,

$$N(E, k_+) = -\sum_{n=0,1} \mathrm{Im}\mathrm{Tr}\hat{\mathscr{G}}(E, k_+)_{n,n},$$

where $\hat{\mathscr{G}}(E, k_+)_{n,n'}$ is the local Green function at the interface with $n, n' = 0, 1$, and the trace is over the spin and orbital space. In the tunneling (weak coupling, small J) limit, the interface spectrum includes a sharply defined Dirac cone as on the surface of TI. As J is increased, the linearly dispersing mode becomes ill defined and eventually replaced by a continuum of metal induced gap states.

Once the lattice Green function is known for given incident E and $k_\parallel$, the scattering (reflection) matrix can be constructed from $\hat{\mathscr{G}}$ by [30],

$$\hat{S}(E, k_+) = \hat{\mathscr{G}}(E, k_+)_{0,0} g_M^{-1}(E, k_+) - \hat{1}$$

where g_M is the spin-degenerate bulk Green function of metal. Fig. 5 shows the evolution of $|g(\theta)|$ and $\alpha(\theta)$ for increasing J, where a level broadening of $E/10$ is used. Most importantly, we observe that the existence of a critical angel θ_c, where complete spin-flip occurs and α jumps by π, is a robust phenomenon. It is independent of the details of the contact, the metal Fermi surface, or other high energy features in the band structure.

To understand the perfect spin flip, we first focus on the tunneling limit, $J \ll t_M$. In this limit, the local spectrum at layer $n = 1$ as shown in the right panel of Fig. 4 approaches the TI surface spectrum, namely the helical Dirac cone. An incident up spin tunneling across the barrier will develop resonance with the helical mode, which is a quasi-stationary state with long life time, if its momentum and energy satisfy $k_\parallel = E/A_2$. Moreover, it has to flip its spin, since only down spin can propagate in the k_x direction (suppose $k_y = 0$). The π jump in the phase shift is also characteristic of the resonance. Indeed, we have checked that precisely at θ_c the resonance criterion, $k_f \sin\theta_c = E/A_2$, is met. We also varied μ_M for fixed J and t_M, bigger μ_M yields a bigger Fermi surface and a smaller θ_c. This is consistent with the resonance criterion above.

As J is increased, the width of the resonance grows and eventually it is replaced by a broad peak (dip) in $|f|$ ($|g|$), but the vanishing of $|g|$ and π shift in α at θ_c persist to good contacts, even though in this limit the interface is flooded by MIGS (left panel of Fig. 4) and bears little resemblance to the Dirac spectrum. With all other parameters held fixed, θ_c increases with J. Qualitatively,

coupling to TI renormalizes the metal spectrum near the interface, producing a smaller effective k_f (hence a larger θ_c) compared to its bulk value. It is remarkable that perfect spin flip at the critical angle persists all the way from poor to good contacts. Indeed, the main features observed here for for good contacts using the lattice model agree well with the results obtained in previous section by wave function matching.

2.5 Discussions

We now discuss the experimental implications of our results. The M-TI interface spectrum can be measured by ARPES (or scanning tunneling microscope) experiments on metal film coated on a topological insulator. Our results also suggest that a topological insulator can serve as a perfect mirror to flip the electron spin in metal. Such spin-active scattering at the M-TI interface may be exploited to make novel spintronic devices. The magnitude of g or f can be measured by attaching two ferromagnetic leads to a piece of metal in contact with TI, forming a multi-terminal device. One of the ferromagnetic leads produces spin-polarized electrons incident on the M-TI interface at some angle, while the other lead detects the polarization of reflected electron, as in a giant magneto-resistance junction. The spin rotation angle α can be measured indirectly by comparing the predicted current-voltage characteristics of M-TI-M or Superconducto-TI-Superconductor junctions, which are sensitive the phase shift α. It can also be inferred from the spin transport in a TI-M-TI sandwich, as discussed for QSH insulator in Ref. [2]. Detailed calculations of the transport properties of these structured, using the scattering matrix obtained here, will be subjects of future work.

Chapter 3

Superconducting Proximity Effect

We present microscopic, self-consistent calculations of the superconducting order parameter and pairing correlations near the interface of an s-wave superconductor and a three-dimensional topological insulator with spin-orbit coupling. We discuss the suppression of the order parameter by the topological insulator and show that the equal-time pair correlation functions in the triplet channel, induced by spin-flip scattering at the interface, are of $p_x \pm ip_y$ symmetry. We verify that the spectrum at sub-gap energies is well described by the Fu-Kane model. The sub-gap modes are viewed as interface states with spectral weight penetrating well into the superconductor. We extract the phenomenological parameters of the Fu-Kane model from microscopic calculations, and find they are strongly renormalized from the bulk material parameters. This is consistent with previous results of Stanescu et al for a lattice model using perturbation theory in the tunneling limit.

3.1 Introduction

Fu and Kane showed that at the interface between a three-dimensional topological band insulator (TI) and an s-wave superconductor (S) forms a remarkable two-dimensional non-Abelian superconductor [31]. It hosts Majorana zero modes at vortex cores, as in a $p_x + ip_y$ superconductor [32], but respects time-reversal symmetry. As argued in Ref. [31], the presence of superconductor induces a pairing interaction between the helical Dirac fermions at the surface of the topological insulator, and gaps out the surface spectrum. Then, the interface can be modeled elegantly by a simple matrix Hamiltonian in Nambu space (we follow the convention of Ref. [33]),

$$H_{FK}(\mathbf{k}) = \begin{pmatrix} h_s(\mathbf{k}) & i\sigma_y\Delta_s \\ -i\sigma_y\Delta_s^* & -h_s^*(-\mathbf{k}) \end{pmatrix}, \tag{3.1}$$

where $\mathbf{k} = (k_x, k_y)$ is the two-dimensional momentum in the interface plane, σ_i are the Pauli matrices, $h_s(\mathbf{k})$ is the surface Hamiltonian for the topological insulator describing the helical Dirac fermions [33, 16],

$$h_s(\mathbf{k}) = -\mu_s + v_s(\sigma_x k_y - \sigma_y k_x). \tag{3.2}$$

Fu and Kane also proposed to use S-TI proximity structures to generate and manipulate Majorana fermions which obey non-Abelian statistics and are potentially useful for fault tolerant quantum computation [31]. This proposal and a few others that followed based on superconductor-semiconductor heterostructures [34, 35, 1, 36, 37] have revived the interest in superconducting proximity effect involving insulating/semiconducting materials with spin-orbit coupling. More complex

S-TI proximity structures with ferromagnets [38, 39] or unconventional superconductors [40] have been investigated.

Experiments are beginning to realize various S-TI proximity structures [41, 42, 43]. In light of these developments, it is desirable to understand to what extent the effective model H_{FK} holds, and what are the values of (Δ_s, μ_s, v_s) for given materials. Answering these questions is crucial for future experiments designed to probe and manipulate Majorana fermions. As a first step in this direction, Stanescu et al considered a microscopic lattice model for the TI-S interface [19]. In this model, TI and S are described by a tight binding Hamiltonian defined on the diamond and hexagonal lattice respectively. The two materials are coupled by tunneling term in the Hamiltonian. These authors found that for small $\mathbf{k}$, $H_{FK}(\mathbf{k})$ is valid but its parameters are significantly renormalized by the presence of the superconductor. This is supported by leading order perturbation theory in the weak coupling (tunneling) limit. They also discussed the induced p-wave correlation within the framework of perturbation theory. The p-wave correlation has also been noted in an analogous proximity structure in two dimension between a quantum spin Hall insulator and a superconductor [44].

In this work, we consider S-TI proximity structures where S and TI are *strongly* coupled to each other, rather than being separated by a tunneling barrier. This is the desired, presumably the optimal, configuration to realize the Fu-Kane proposal, e.g. to achieve maximum value of Δ_s in H_{FK} for given superconductor. In the strong coupling limit, the modification of superconductivity by the TI becomes important. This includes the suppression of the superconducting order parameter, the induction of triplet pair correlations by spin-active scattering at the interface, and the formation of interface states below the bulk superconducting gap. In order to accurately answer questions raised in the preceding paragraph for strongly coupled S-TI structures, one has to self-consistently determine the spatial profile of the order parameter near the interface.

Our work is also motivated by recent experimental discovery that Copper-doped topological insulator $Cu_xBi_2Se_3$ becomes superconducting at a few Kelvins [45, 46, 47]. It seems possible then to combine such superconductors with topological insulator Bi_2Se_3 to achieve strong proximity coupling. We set up microscopic, continuum models for the S-TI structures and solve the result Bogoliubov-de Gennes (BdG) equation numerically. We first compute the superconducting order parameter as a function of the distance away from the interface. We then verify the validity of the Fu-Kane effective model and extract its parameters from the low energy sector of the energy spectrum. The emergence of H_{FK} will be viewed as the result of the "inverse proximity effect", namely strong modification of superconductivity by the presence of TI. This is in contrast to the previous viewpoint of pairing between surface Dirac fermions, which is a more proper description in the tunneling limit. The spectral weight of these low energy modes (with energy below the bulk superconducting gap) are shown explicitly to peak near the interface but penetrate well into the superconductor. We will also show analytically that the induced triplet pair correlations are of $p_x \pm ip_y$ orbital symmetry, and systematically study their spatial and momentum dependence. Our results connect the phenomenological theory of Fu and Kane [31] to real materials. Our results for continuum models and strong coupling limit are also complementary to the results of Stanescu et al [19] for lattice models and tunneling limit.

In what follows, we first outline the formulation of the problem and then present the main results. Technical details on numerically solving the BdG equation are relegated to the appendix.

3.2 Model and Basic Equations

The band gaps of topological insulators are much larger than the superconducting gap of all weak coupling s-wave superconductors. For the purpose of studying the proximity effect between such superconductors and topological insulators, it is sufficient to describe the topological insulator using the low energy effective $\mathbf{k}\cdot\mathbf{p}$ Hamiltonian. Following Zhang et al [48], we model Bi_2Se_3 by

$$H_{TI}(\mathbf{k}) = \begin{pmatrix} M(\mathbf{k}) & 0 & A_1k_z & A_2k_- \\ 0 & M(\mathbf{k}) & A_2k_+ & -A_1k_z \\ A_1k_z & A_2k_- & -M(\mathbf{k}) & 0 \\ A_2k_+ & -A_1k_z & 0 & -M(\mathbf{k}) \end{pmatrix} - \mu\hat{I}. \tag{3.3}$$

Here $k_\pm = k_x \pm ik_y$, $M(\mathbf{k}) = M - B_1k_z^2 - B_2(k_x^2+k_y^2)$, and $\hat{I}$ is 4×4 unit matrix. The numerical values of the parameters are obtained from first principle calculations [48, 49], $M = 0.28$ eV, $A_1 = 2.2$ eVÅ, $A_2 = 4.1$ eVÅ, $B_1 = 10$ eVÅ^2, $B_2 = 56.6$ eVÅ^2. We work in basis $\{|1\uparrow\rangle, |1\downarrow\rangle, |2\uparrow\rangle, |2\downarrow\rangle\}$, where 1 (2) labels the $P1_z^+$ ($P2_z^+$) orbital [48]. Note that we have neglected the unimportant diagonal term $\epsilon_0(\mathbf{k})$ in Ref. [48] which only slightly modifies the overall curvature of the band dispersion. We also keep the chemical potential μ as a tuning parameter.

We consider a simple model of superconductor derived from a metallic state obtained by turning off the spin-orbit coupling ($A_1 = A_2 = 0$) in H_{TI} and tuning the Fermi level well into the conduction band [50]. The metal Hamiltonian

$$H_M(\mathbf{k}) = \mathrm{diag}[M(\mathbf{k}), M(\mathbf{k}), -M(\mathbf{k}), -M(\mathbf{k})] - E_f\hat{I}, \tag{3.4}$$

with $E_f > M$. This mimics electron-doping the topological insulator [46] or equivalently electrochemically shifting its chemical potential by applying a gate voltage [21]. As shown in Fig. 3.1, the valence band (band 1 with dispersion $M(\mathbf{k}) - E_f$) is well below the Fermi level and remains inert as far as superconductivity is concerned. Next, within the framework of Bardeen-Cooper-Schrieffer theory, we assume attractive interaction between the electrons in the conduction band (band 2) near the Fermi surface described by the reduced Hamiltonian,

$$H_{int} = \sum_{\mathbf{k}} \psi_{2\uparrow}^\dagger(\mathbf{k})\psi_{2\downarrow}^\dagger(-\mathbf{k})\Delta + h.c. \tag{3.5}$$

Here Δ is the superconducting order parameter, $\psi_{l\sigma}^\dagger$ is the electron creation operator for orbital $l = 1, 2$ and spin $\sigma = \uparrow, \downarrow$. The superconductor is then described by

$$H_S = \sum_{\mathbf{k},l,\sigma} \psi_{l\sigma}^\dagger(\mathbf{k})H_M(\mathbf{k})_{l\sigma,l\sigma}\psi_{l\sigma}(\mathbf{k}) + H_{int}. \tag{3.6}$$

Note that H_S and H_{TI} are in the same basis.

This model can serve as a generic model for s-wave superconductors with negligible spin-orbital coupling. Whether it can actually describe the superconductor $Cu_xBi_2Se_3$ has to be settled by future experiments. The transition temperature of $Cu_xBi_2Se_3$ at optimal doping $x = 0.12$ is $T_c = 3.8$K, which corresponds to a zero temperature superconducting gap $\Delta \sim 0.6$meV [45, 46, 47]. The Fermi level is 0.25eV above the bottom of the conduction band, and the Fermi wave vector $k_f \sim 0.12$Å^{-1}. The pairing symmetry of $Cu_xBi_2Se_3$ is to our best knowledge is unknown at present (it appears to be fully gapped from the specific heat measurement [47] and might be a topological superconductor [46]). If it turns out to be a conventional s-wave superconductor, its mains features will be captured by H_S above with suitable choice of E_f and Δ.

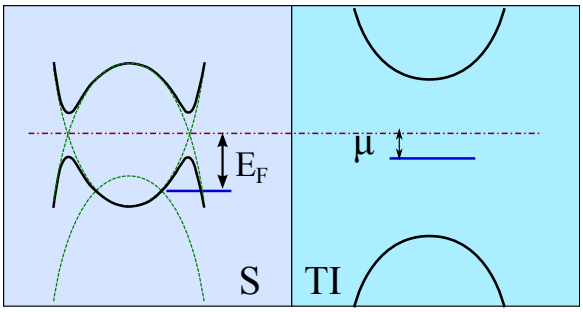

Figure 3.1: Schematic (not to scale) band diagrams in a superconductor-topological insulator (S-TI) proximity structure. E_f is the Fermi energy of the metal described by H_M measured from the band crossing point. μ is the chemical potential of TI measured from the band gap center. The superconducting gap is much smaller than the band gap of TI.

Now consider a proximity structure consisting of a superconductor at $z < d$ and a topological insulator at $z > d$ (Fig. 3.1). The interface at $z = d$ is assumed to be specular, so the momentum $\mathbf{k}_\parallel = (k_x, k_y)$ parallel to the interface is conserved. The Hamiltonian for the whole system

$$\begin{aligned}\mathcal{H} = \int d\mathbf{k}_\parallel dz \Big\{ & \sum_\sigma \psi^\dagger_{1\sigma}(\mathbf{k}_\parallel, z)[h_0 - \mu(z)]\psi^\dagger_{1\sigma}(\mathbf{k}_\parallel, z) \\ & - \sum_\sigma \psi^\dagger_{2\sigma}(\mathbf{k}_\parallel, z)[h_0 + \mu(z)]\psi^\dagger_{2\sigma}(\mathbf{k}_\parallel, z) \\ & + \Delta(z)\psi^\dagger_{2\uparrow}(\mathbf{k}_\parallel, z)\psi^\dagger_{2\downarrow}(-\mathbf{k}_\parallel, z) + h.c. \\ & + A_1(z)[\psi^\dagger_{1\uparrow}(-i\partial_z)\psi_{2\uparrow} + \psi^\dagger_{1\downarrow}(i\partial_z)\psi_{2\downarrow} + h.c.] \\ & + A_2(z)[\psi^\dagger_{1\uparrow}k_-\psi_{2\downarrow} + \psi^\dagger_{1\downarrow}k_+\psi_{2\uparrow} + h.c.]\Big\}. \end{aligned} \tag{3.7}$$

Here $h_0(\mathbf{k}_\parallel, \partial_z) = M - B_1\partial_z^2 - B_2 k_\parallel^2$, $\mu(z)$ and $A_i(z)$ are piece-wise constant,

$$\mu(z) = E_f\theta(d - z) + \mu\theta(z - d), \tag{3.8}$$

$$A_i(z) = A_i\theta(z - d), \quad i = 1, 2 \tag{3.9}$$

in terms of the step function θ. The order parameter obeys the gap equation

$$\Delta(z) = g(z)\int d\mathbf{k}_\parallel \langle\psi_{2\uparrow}(\mathbf{k}_\parallel, z)\psi_{2\downarrow}(-\mathbf{k}_\parallel, z)\rangle. \tag{3.10}$$

We assume $g(z) = g\theta(d - z)$, the coupling constant g determines the bulk gap.

To self-consistently solve Eq. (3.7) and (3.10), we introduce Bogoliubov transformation

$$\psi_{l\sigma}(\mathbf{k}_\parallel, z) = \sum_n u_{n,l\sigma}(\mathbf{k}_\parallel, z)\gamma_{n,\mathbf{k}_\parallel} + v^*_{n,l\sigma}(\mathbf{k}_\parallel, z)\gamma^\dagger_{n,\mathbf{k}_\parallel} \tag{3.11}$$

to diagonalize $\mathcal{H}$ as

$$\mathcal{H} = E_g + \int d\mathbf{k}_\parallel \sum_n \epsilon_n(k_\parallel)\gamma^\dagger_{n,\mathbf{k}_\parallel}\gamma_{n,\mathbf{k}_\parallel}, \tag{3.12}$$

where E_g is the ground state energy, and $\gamma^\dagger_{n,\mathbf{k}_\parallel}$ is the creation operator of Bogoliubov quasiparticles with energy $\epsilon_n(k_\parallel)$. The wave function u and v satisfy the following Bogliubov-de Gennes (BdG) equation,

$$\hat{H}_B(\mathbf{k}_\parallel, z)\hat{\phi}_n(\mathbf{k}_\parallel, z) = \epsilon_n(k_\parallel)\hat{\phi}_n(\mathbf{k}_\parallel, z). \tag{3.13}$$

Here, the BdG Hamiltonian

$$\hat{H}_B = \begin{pmatrix} h_0 - \mu & \mathbf{d}\cdot\boldsymbol{\sigma} & 0 & 0 \\ \mathbf{d}\cdot\boldsymbol{\sigma} & -h_0 - \mu & 0 & -\Delta\, i\sigma_y \\ 0 & 0 & \mu - h_0 & \mathbf{d}\cdot\boldsymbol{\sigma}^* \\ 0 & \Delta^*\, i\sigma_y & \mathbf{d}\cdot\boldsymbol{\sigma}^* & \mu + h_0 \end{pmatrix}, \tag{3.14}$$

and the wave function (dropping the arguments)

$$\hat{\phi}_n = (u_{n,1\uparrow}, u_{n,1\downarrow}, u_{n,2\uparrow}, u_{n,2\downarrow}, v_{n,1\uparrow}, v_{n,1\downarrow}, v_{n,2\uparrow}, v_{n,2\downarrow})^{\mathrm{T}}. \tag{3.15}$$

The vector $\mathbf{d}(\mathbf{k}_\parallel, z)$ is defined as

$$d_x = A_1(z)k_x,\ d_y = A_1(z)k_y,\ d_z = A_2(z)(-i\partial_z). \tag{3.16}$$

Other quantities such as $h_0(\mathbf{k}_\parallel, z)$, $\mu(z)$, and $\Delta(z)$ are defined above. In terms of the wave functions, the zero temperature gap equation becomes

$$\Delta(z) = g(z)\int d\mathbf{k}_\parallel \sum_n{}' u_{n,2\uparrow}(\mathbf{k}_\parallel, z)v^*_{n,2\downarrow}(-\mathbf{k}_\parallel, z), \tag{3.17}$$

where the summation denoted by prime is restricted to $0 < \epsilon_n < \omega_D$ with ω_D being the Debye frequency.

We will exploit a particular symmetry of the BdG Hamiltonian to simplify calculations. Define the polar angle φ_k for the in-plane wave vector $\mathbf{k}_\parallel$,

$$k_x + ik_y = k_\parallel e^{i\varphi_k}. \tag{3.18}$$

Then the BdG Hamiltonian for arbitrary (k_x, k_y) is related to that for $(k_x = k_\parallel, k_y = 0)$ by unitary transformation

$$\hat{U}^\dagger(\mathbf{k}_\parallel)\hat{H}_B(k_x, k_y)\hat{U}(\mathbf{k}_\parallel) = \hat{H}_B(k_\parallel, 0). \tag{3.19}$$

Here U is a block diagonal matrix,

$$U(\mathbf{k}_\parallel) = \mathrm{diag}[e^{-i\sigma_z\frac{\varphi_k}{2}}, e^{-i\sigma_z\frac{\varphi_k}{2}}, e^{i\sigma_z\frac{\varphi_k}{2}}, e^{i\sigma_z\frac{\varphi_k}{2}}]. \tag{3.20}$$

Thus, the eigen energy ϵ_n only depends on the magnitude of $\mathbf{k}_\parallel$. Once the wave function for $\varphi_k = 0$ is known, the wave function for $\varphi_k \in (0, 2\pi)$ can be obtained by simple unitary transformation.

We solve the matrix differential equation (3.13) by conserving it into an algebraic equation, following the treatment of superconductor-ferromagnet structure by Halterman and Valls [51]. The whole S-TI proximity structure is assumed to have finite dimension L in the z direction. The superconductor occupies the region $0 < z < d$, while the topological insulator occupies $d < z < L$. Hard wall boundary conditions are enforced at the end points, $z = 0$ and $z = L$. The exact boundary conditions at the end points only affect the local physics there, provided that the boundaries are sufficiently far away from the S-TI interface. We expand the wave function and order parameter in Fourier series [51],

$$u_{n,l\sigma}(z) = \sum_m u^{l\sigma}_{nm}\,\phi_m(z), \tag{3.21}$$

$$v_{n,l\sigma}(z) = \sum_m v^{l\sigma}_{nm}\,\phi_m(z), \tag{3.22}$$

$$\Delta(z) = \sum_m \Delta_m\,\phi_m(z), \tag{3.23}$$

$$\phi_m(z) = \sqrt{2/L}\sin(k_m z). \tag{3.24}$$

The integer $m = 1, 2, ..., N$ labels the quantized longitudinal (along z) momentum $k_m = m\pi/L$. The cutoff N is chosen as [52]

$$B_1 k_N^2 = M + E_f + \omega_D. \tag{3.25}$$

By expansion Eq. (3.21)-(3.23), the BdG equation becomes an $8N \times 8N$ matrix equation. With a reasonable guess of the order parameter profile, the eigen energies and eigen wave functions are obtained by solving the matrix eigen value problem. Then a new order parameter profile is computed from the gap equation. The procedure is iterated until convergence is achieved. Relevant technical details can be found in the Fourier calculations section.

To analyze the spectrum of the system, it is convenient to define the retarded Green's function

$$G_{l\sigma}^R(\mathbf{k}_\parallel, z, t) = -i\theta(t)\langle\{\psi_{l\sigma}(\mathbf{k}_\parallel, z, t), \psi_{l\sigma}^\dagger(\mathbf{k}_\parallel, z, 0)\}\rangle \tag{3.26}$$

where the time-dependent field operators are in Heisenberg picture. For given $\mathbf{k}_\parallel$ and z, the spectral functions are defined as

$$N_{l\sigma}(\mathbf{k}_\parallel, z, \omega) = -\mathrm{Im}G_{l\sigma}^R(\mathbf{k}_\parallel, z, \omega), \tag{3.27}$$

$$N(\mathbf{k}_\parallel, z, \omega) = \sum_{l\sigma} N_{l\sigma}(\mathbf{k}_\parallel, z, \omega). \tag{3.28}$$

In terms of the wave functions and eigen energies,

$$N_{l\sigma}(\mathbf{k}_\parallel, z, \omega > 0) = \sum_n |u_{n,l\sigma}(\mathbf{k}_\parallel, z)|^2 \delta(\omega - \epsilon_n). \tag{3.29}$$

We also introduce the equal-time pair correlation functions for the conduction electrons

$$F_{\alpha\beta}(\mathbf{k}_\parallel, z) = \langle\psi_{2\alpha}(\mathbf{k}_\parallel, z)\psi_{2\beta}(-\mathbf{k}_\parallel, z)\rangle. \tag{3.30}$$

For example, at zero temperature we have

$$F_{\uparrow\uparrow}(\mathbf{k}_\parallel, z) = \sum_n{}' u_{n,2\uparrow}(\mathbf{k}_\parallel, z) v_{n,2\uparrow}^*(-\mathbf{k}_\parallel, z), \tag{3.31}$$

$$F_{\downarrow\downarrow}(\mathbf{k}_\parallel, z) = \sum_n{}' u_{n,2\downarrow}(\mathbf{k}_\parallel, z) v_{n,2\downarrow}^*(-\mathbf{k}_\parallel, z). \tag{3.32}$$

Triplet components of F will be induced near the S-TI interface by spin-active scattering [50].

3.3 Fourier Expansion

We follow the numerical scheme of Halterman and Valls to solve the matrix BdG equation [51]. The wave functions and the order parameter are expanded in the orthonormal basis $\{\phi_m(z)\}$, with $m = 1, ..., N$. For example, function $u_{n,1\uparrow}(z)$ is represented by N numbers,

$$(u_{n,1}^{1\uparrow}, u_{n,2}^{1\uparrow}, ...u_{n,m}^{1\uparrow}..., u_{n,N}^{1\uparrow}).$$

Accordingly, each term in $\hat{H}_B$ is represented by a $N \times N$ matrix with the matrix elements given by

$$\begin{aligned} h_0(\mathbf{k}_\parallel, \partial_z) &\to \delta_{mm'}(M - B_1 k_m^2 - B_2 k_\parallel^2) \\ U(z) &\to E_f E_{mm'} + \mu F_{mm'} \\ A_2(z)\partial_z &\to A_2 G_{mm'} \\ A_1(z)k_\pm &\to A_z k_\pm F_{mm'} \\ \Delta &\to D_{mm'} \equiv \sum_{m''} J_{m,m',m''}\Delta_{m''} \end{aligned}$$

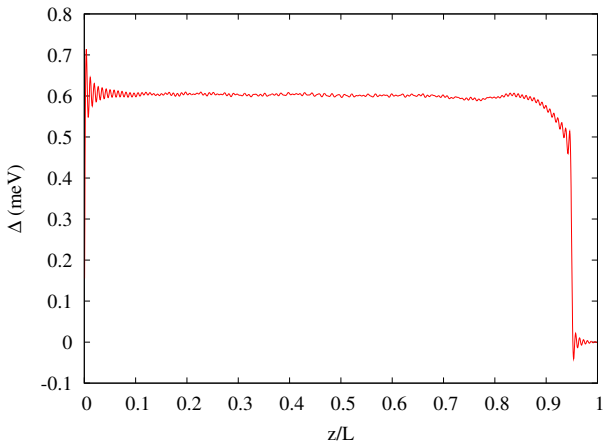

Figure 3.2: The superconducting order parameter $\Delta(z)$ near an S-TI interface at $z = d = 0.95L$. The superconductor occupies $0 < z < d$, and topological insulator occupies $d < z < L$. $L = 300$ nm, μ=0, the bulk gap Δ_0 =0.6meV.

where

$$E_{mm'} = \int_0^d \phi_m(z)\,\phi_{m'}(z)dz$$
$$F_{mm'} = \int_d^L \phi_m(z)\,\phi_{m'}(z)dz$$
$$G_{mm'} = \int_d^L \phi_m(z)\partial_z\phi_{m'}(z)dz$$
$$J_{m,m',m''} = \int_0^d \phi_m(z)\,\phi_{m'}(z)\,\phi_{m''}(z)dz$$

These integrals can be evaluated analytically. Then the BdG equation becomes an $8N \times 8N$ matrix equation. The gap equation can be rewritten as

$$\Delta_m = g \int d\mathbf{k}_\parallel \sum_n{}' \sum_{m',m''} J_{m,m',m''} u^{2\uparrow}_{nm'}(\mathbf{k}_\parallel) v^{2\downarrow}_{nm''}(-\mathbf{k}_\parallel)^*$$

The integral over $\mathbf{k}_\parallel$ is first simplified to an integral over $k_\parallel$ by the symmetry Eq. (3.19) and then evaluated numerically with high momentum cutoff $\sqrt{(E_F + \omega_D + M)/B_2}$.

3.4 The Order Parameter

First we present the spatial profile of the superconducting order parameter $\Delta(z)$ after the convergence is achieved. In all following calculations, E_f is fixed at 0.4eV, which is modeled after optimally doped $Cu_xBi_2Se_3$ [46]. And the Debye frequency is set as $\omega_D = 0.1E_f$ [51]. Fig. 3.2 shows an example with $\mu = 0$, $L = 300$nm, $d = 0.95L$, and a bulk gap of 0.6meV as found in $Cu_xBi_2Se_3$. Going from the superconductor into the topological insulator, Δ first gets suppressed as the interface is approached before it drops to zero inside TI. The suppression is roughly 20% at the interface. Note that the fine wiggles of Δ in the simulation results are due to the finite

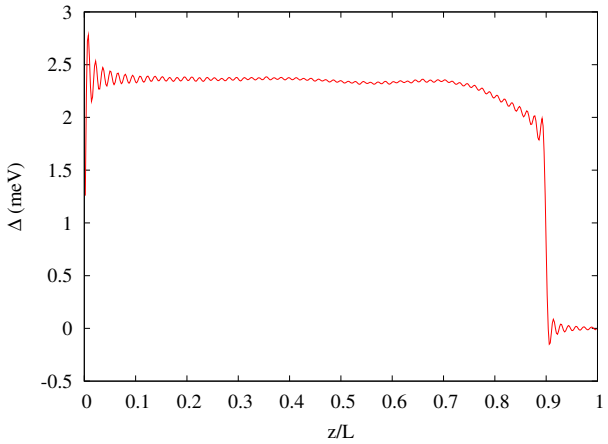

Figure 3.3: The order parameter $\Delta(z)$ near an S-TI interface at $z = d = 0.9L$. $L = 160$ nm, μ=0, $\Delta_0 \sim 2.4$meV.

momentum cutoff of the longitudinal momentum k_m. As previously discussed by Stojkovic and Valls [52], the number of oscillations is $\sim N/2$, and the oscillation amplitude vanishes in the bulk as N is increased. In this case, N is chosen to be 258 according to Eq. (3.25). So the matrix to be diagonalized is 2064 by 2064.

Fig. 3.3 show the result for $\mu = 0$, $d = 0.9L$, and a superconductor with bulk gap $\Delta_0 \sim 2.4$meV. Since the coherence length is much smaller than the previous example, it is sufficient to consider $L = 160$nm, and correspondingly $N = 138$. The order parameter profile depends weakly on μ, as shown in Fig. 3.4 for a superconductor with bulk gap ~ 5.2meV. From these examples, one observes that the length scale over which Δ is significantly suppressed does *not* scale with ξ_0, the zero temperature coherence length of the superconductor. Rather it stays roughly the same, on the order of 30nm, as ξ_0 is varied over one decade from Fig. 3.2 to Fig. 3.4 (note the horizontal axis is z/L). This is not very surprising since ξ_0 is not the only length scale at play here. The interface represents a strong (as compared to Δ_0) perturbation that significantly distorts the bulk wave functions. The self-consistent microscopic BdG approach provides a reliable way to capture the details of $\Delta(z)$ near the interface.

It is illuminating to compare the proximity effect in S-TI structure with that in S-F structure [53], where F stands for a ferromagnetic insulator. The presence of F breaks time-reversal and spin rotation symmetry and significantly suppresses the order parameter. The suppression is sensitive to the spin mixing angle which is related to the band gap and exchange field of F [53]. In contrast, despite the spin-active scattering of electrons by TI which introduces spin-flips and spin-dependent phase shifts [50], spin-orbit coupling is not pair breaking. The suppression of Δ near the interface is to a large extent due to the reorganization of local wave functions enforced by the boundary conditions at $z = d$ for piece-wise potentials $\mu(z)$, $A_i(z)$, $g(z)$. It depends on for example how the wave functions decay inside the TI for given E_f and μ, and involves "high-energy" physics beyond the scale of Δ but below the scale of the band gap. To test this, we have investigated the proximity effect between the same superconductor and a hypothetical ordinary insulator modeled by H_{TI} with $A_1 = A_2 = 0$ and the same band gap. The suppression of Δ by such an ordinary insulator turns out to be very similar.

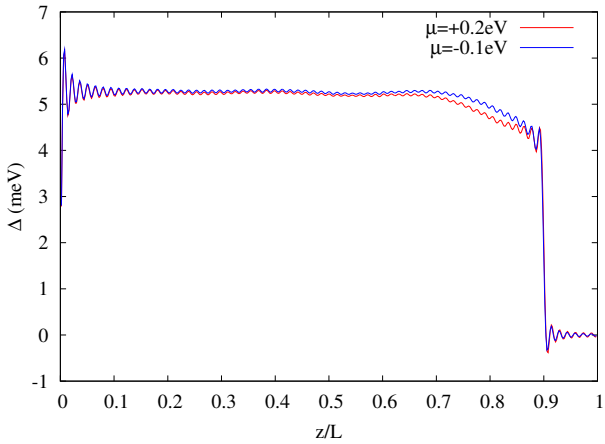

Figure 3.4: The order parameter profile for two different chemical potentials of the topological insulator, $\mu = -0.1$eV and $\mu = 0.2$eV. $L = 160$nm, $\Delta_0 \sim 5.2$meV.

3.5 The Interface Mode and the Fu-Kane Model

Next we analyze the energy spectrum of the system, $\epsilon_n(k_\parallel)$, obtained from the BdG calculation. Take the case of $\mu = 0$, $L = 160$nm, $d = 0.9L$, $\Delta_0 \sim 5.2$meV as an example. Fig. 3.5 shows the first several energy levels of the composite system versus the transverse momentum $k_\parallel$. There are many continuously dispersing modes at energies above the bulk gap. They are the usual Bogoliubov quasiparticles for different quantized longitudinal momenta. One also sees a series of avoided level crossings. At small $k_\parallel$ emerges a well-defined mode below Δ_0. We will identify it as the interface mode first discussed by Fu and Kane [31].

The Fu-Kane model Eq. (4.12) predicts the dispersion

$$E(k) = \sqrt{|\Delta_s|^2 + (v_s k \pm \mu_s)^2}. \tag{3.33}$$

We fit the very low energy portion of the spectrum to this prediction to extract the phenomenological parameters in the Fu-Kane model. The result is shown in Fig. 3.5. We find that, not surprisingly, $\Delta_s = 1.8$meV which is much smaller than $\Delta_0 = 5.2$meV, and $v_s = 2.7$eVÅ which deviates significantly from $A_2 = 4.2$eVÅ predicted for the surface dispersion of TI. Moreover, $\mu_s = 7.5$meV despite that the chemical potential of TI is $\mu = 0$. Therefore, our results show that the values of (Δ_s, v_s, μ_s) are strongly renormalized by the presence of the superconductor. This is consistent with the findings of Stanescu et al for weakly coupled S-TI structures [19].

We have checked the validity of the Fu-Kane model for a variety of chemical potentials. Representative examples are plotted in Fig. 3.6. In each case, the sub-gap mode can be well accounted by the Fu-Kane model with suitable choice of parameters. While μ_s is always different from μ, numerically we find it scales linearly with μ. At the same time, Δ_s and v_s show no strong dependence on μ for this set of parameters. To make sure that the sub-gap mode is indeed localized near the interface, we plot in Fig. 3.7 the z dependence of the spectral function $N(k_\parallel, z, \omega)$. The spectral weight of the sub-gap mode is peaked near the interface and decays over a length scale $\sim \xi_0$ into the superconductor. This result clearly shows that for strongly coupled S-TI interfaces, the Fu-Kane model actually describe a rather "fat" interface mode. Note that the spectral weight on the TI side (not shown in the figure) is finite, but it is much smaller in magnitude and decays very fast inside TI. Finally, Fig. 3.8 shows the local density of states near the interface. The interface mode leads to finite density of states below the bulk gap, but the spectral weight is very small.

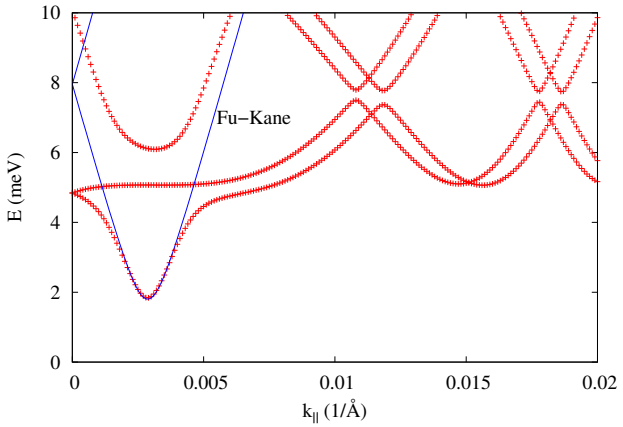

Figure 3.5: The lowest few energy levels $\epsilon_n(k_\parallel)$. $\mu = 0$, $L = 160$nm, and the bulk superconducting gap Δ_0 ∼5.2meV. A well-defined interface mode is clearly visible at sub-gap energies. Solid lines show a fit to the Fu-Kane model, with $\Delta_s = 1.8$meV, $v_s = 2.7$eVÅ, and $\mu_s = 7.5$meV.

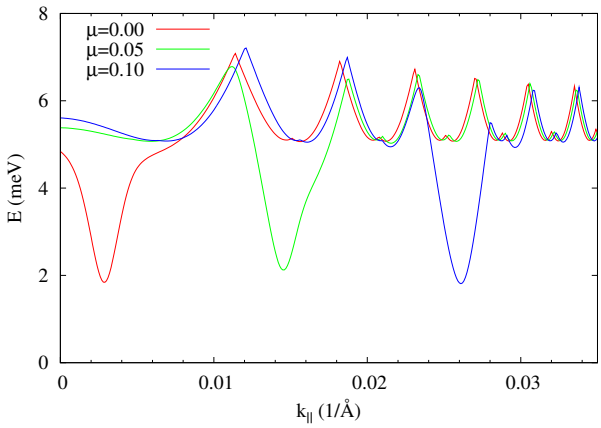

Figure 3.6: The dispersion of the lowest energy level for different μ (in eV). Other parameters are the same as in Fig. 3.5, $L = 160$nm and Δ_0 ∼5.2meV. Fu-Kane model well describes the lowest energy mode. As μ is increased, Δ_s and v_s stay roughly the same, while μ_s scales linearly with μ.

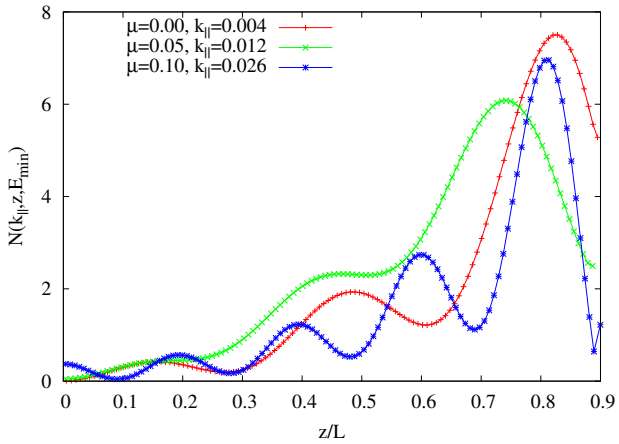

Figure 3.7: The spectral function $N(k_{\|}, z, \omega)$ of the lowest energy level, $\omega = E_{min}$, shown in Fig. 3.6. The interface is at $z = 0.9L$, L=160nm. The spectral function oscillates rapidly with z, so only its envelope is plotted.

We have carried out similar analysis for superconductors with larger coherence length. Fig. 3.9 shows the evolution of the sub-gap mode with μ for $\Delta_0 = 2.4$meV. In this case, the values of (Δ_s, v_s, μ_s) all varies with μ. Superconductors with larger ξ_0 and smaller Δ_0 are thus more sensitive to changes in μ and other microscopic details near the interface. The exact values of the effective parameters in the Fu-Kane model in general depend on such microscopic details.

3.6 Triplet Pair Correlations

It is well known that in heterostructures of s-wave superconductors, pairing correlations in other orbital channels, e.g. p-wave correlations, will be induced by scattering at the interfaces [54, 55]. For example, inversion/reflection symmetry ($z \leftrightarrow -z$) is lost in an S-TI proximity structure, and the appearance of p-wave correlations seems natural from partial wave analysis. Moreover, scattering by a topological insulator is spin-active. The spin-orbit coupling inside a TI acts like a momentum-dependent magnetic field to flip the electron spin and introduce different phase shifts for spin up and down electrons. The scattering matrix has been worked out by us previously [50]. Thus, a singlet s-wave Cooper pair can be converted into a pair of electrons in spin-triplet state at the S-TI interface. However, it is important to recall that by assumption attractive interaction only exists (or is appreciable) in the s-wave channel. There is no binding force to sustain a triplet Cooper pair or a triplet superconducting order parameter. Similar (but different) pairing correlations in superconductor-ferromagnet hybrid structures have been extensively studied [54]. The appearance of p-wave correlations in S-TI systems has been pointed out previously by Stanescu et al using a perturbative analysis [19].

We focus on the equal-time pair correlation functions defined in Eq. (3.30). By exploiting the symmetry of the BdG Hamiltonian, Eq. (3.19), we are able to find analytically the orbital structure

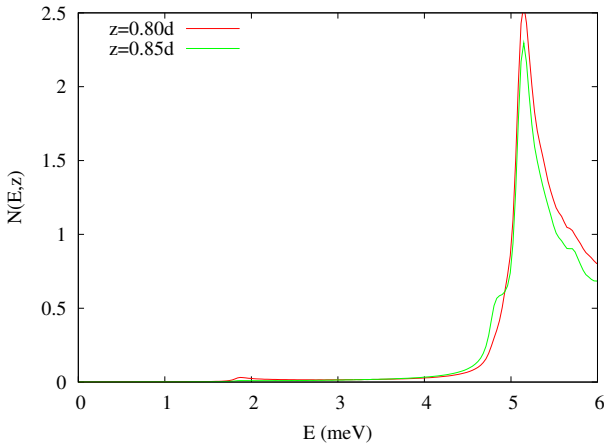

Figure 3.8: The local density of states $N(E, z)$ at $z = 0.8d$ and $z = 0.85d$ (the interface is at $z = 0.9d$). $\mu = 0$, $L = 160$nm, and $\Delta_0 \sim$5.2meV. The subgap states are due to the interface mode. A level broadening $\sim 0.01\Delta_0$ is used.

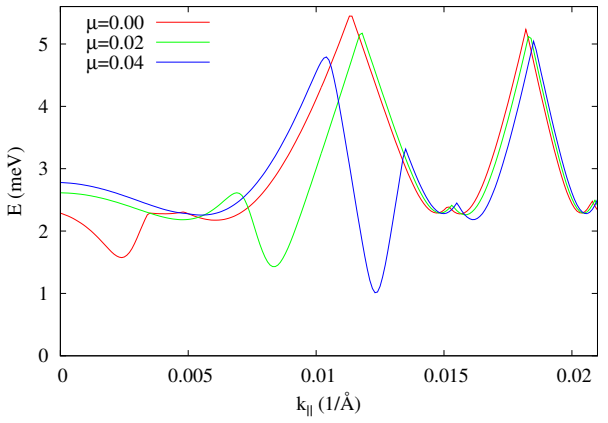

Figure 3.9: The lowest energy level of an S-TI structure with $L = 160$nm, $d = 0.9L$, $\Delta_0 = 2.4$meV. μ is the chemical potential of the TI and measured in eV.

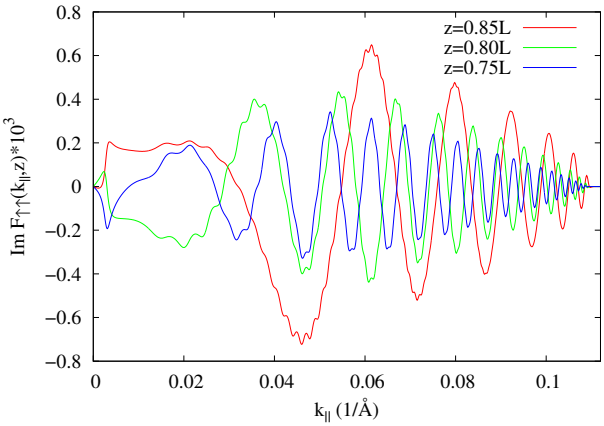

Figure 3.10: The imaginary part of triplet pair correlation function $F_{\uparrow\uparrow}(k_\parallel, z)$. The S-TI interface is at $d = 0.9L$. $\mu = 0$, $L = 160$nm, $\Delta_0 = 5.2$meV.

of the triplet correlation functions. The unitary transformation Eq. (3.20) yields

$$\begin{aligned} u_{2\uparrow}(k_x, k_y) &= u_{2\uparrow}(k_\parallel, 0)e^{-i\varphi_k/2}, \\ u_{2\downarrow}(k_x, k_y) &= u_{2\downarrow}(k_\parallel, 0)e^{+i\varphi_k/2}, \\ v_{2\uparrow}(k_x, k_y) &= v_{2\uparrow}(k_\parallel, 0)e^{+i\varphi_k/2}, \\ v_{2\downarrow}(k_x, k_y) &= v_{2\downarrow}(k_\parallel, 0)e^{-i\varphi_k/2}. \end{aligned} \tag{3.34}$$

Using these relations, we find

$$F_{\uparrow\uparrow}(\mathbf{k}_\parallel, z) = F_{\uparrow\uparrow}(k_\parallel, z)e^{-i\varphi_k}, \tag{3.35}$$

$$F_{\downarrow\downarrow}(\mathbf{k}_\parallel, z) = F_{\downarrow\downarrow}(k_\parallel, z)e^{+i\varphi_k}. \tag{3.36}$$

Namely $F_{\uparrow\uparrow}$ ($F_{\downarrow\downarrow}$) has $p_x - ip_y$ ($p_x + ip_y$) orbital symmetry. Finally, the remaining triplet correlation function

$$\langle \psi_{2\uparrow}(\mathbf{k}_\parallel, z)\psi_{2\downarrow}(-\mathbf{k}_\parallel, z) + \psi_{2\downarrow}(\mathbf{k}_\parallel, z)\psi_{2\uparrow}(-\mathbf{k}_\parallel, z)\rangle \tag{3.37}$$

turns out to be zero. Note that the so-called odd-frequency paring correlations [54, 55, 56], which vanishes in the equal-time limit, are also interesting in S-TI structures, but we will not discuss their behaviors here.

We find that $F_{\uparrow\uparrow}(k_\parallel, z)$ is purely imaginary and identical to $F_{\downarrow\downarrow}(k_\parallel, z)$. The results for $\mu = 0$, $L = 160$nm, $d = 0.9L$, $\Delta_0 = 5.2$meV are plotted in Fig. 3.10. $F_{\uparrow\uparrow}$ vanishes at $k_\parallel = 0$ as well as for large $k_\parallel$, namely when $k_\parallel > \sqrt{(E_F + \omega_D + M)/B_2}$. This is consistent with lack of pairing in both limits. The behavior of $F_{\uparrow\uparrow}$ for small $k_\parallel$ is illustrated in Fig. 3.11 for $\mu = 0$, $L = 300$nm, $d = 0.95L$, $\Delta_0 = 0.6$meV. As comparison, we also plotted the singlet pair correlation function

$$F_{\uparrow\downarrow}(\mathbf{k}_\parallel, z) = \sum_n{}' u_{n,2\uparrow}(\mathbf{k}_\parallel, z)v^*_{n,2\downarrow}(-\mathbf{k}_\parallel, z) \tag{3.38}$$

which is s-wave and purely real.

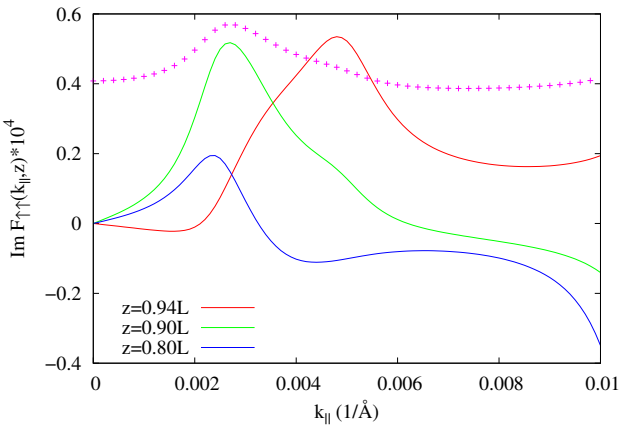

Figure 3.11: The imaginary part of $F_{\uparrow\uparrow}(k_\parallel, z)$. $\mu = 0$, $L = 300$nm, $d = 0.95L$, $\Delta_0 = 0.6$meV. As comparison, the data points show the singlet pair correlation function $F_{\uparrow\downarrow}(k_\parallel, z = 0.9L)/3$.

3.7 Summary

In summary, we have investigated the proximity effect between an s-wave superconductor and a topological insulator using a microscopic continuum model. Strong coupling between the two materials renders the surface state of TI a less useful concept for this problem. Our focus has been on the various modifications to superconductivity by the presence of TI. These include the suppression of the order parameter, the formation of interface modes below the bulk superconducting gap, and the induction of triplet pairing correlations. It is gratifying to see the Fu-Kane effective model emerges in the low energy sector albeit with a set of renormalized parameters. Our results are complementary to previous theoretical work on the proximity effect [31, 19] and confirm the validity of the Fu-Kane model.

We made a few simplifying assumptions in our calculation. The superconductor is described by a two-band model with the valence band well below the Fermi level. Since only electrons near the Fermi surface are relevant for weak coupling superconductivity, we believe our main results are general. As idealizations, the chemical potential, the spin-orbit coupling, and the attractive interaction are assumed to be step functions with a sudden jump at the interface. More elaborate and realistic models can be considered within the framework of BdG equations. For example, one can add a tunneling barrier between S and TI, or include a Rashba-type spin-orbit coupling term (due to the gradient of chemical potential) at the interface. We will not pursuit these generalizations here. Finally, the approach outlined here can be straightforwardly applied to study non-Abelian superconductivity in other superconductor-semiconductor heterostructures where spin-orbit coupling also plays a significant role [34, 35, 1, 36, 37].

Chapter 4

Josephson Junction on TI Surface

4.1 Introduction

The study of topological insulators coupled with a superconductor has attracted much attention recently due to the existence of Majorana particles in such systems. A Majorana particle, paradoxically, is its own antiparticle. It merits study for its implications, an example is Topological Quantum computation.

It has been proposed that an s-wave superconductor inducing superconductivity through proximity effect onto the surface of a TI can be host to Majorana particles in a vortex core at the interface of such a junction [31]. In addition, a Josephson junction can also host Majorana particles, as long as the Josephson phase difference between the two leads of the junction is π [57]. Experimentally, progress has been made to make TI-based Josephson π junctions.

Here, for the first time, we carry out self-consistent calculation of the spectrum and the local density of states of the TI-based Joshephson junctions. These results can be compared to ongoing and future experiments.

4.2 Model and Basic Equations

We start with the physical model of our system as shown in Fig. 4.1. The system is restricted to the 2D surface of the TI where portions of the surface are in contact with S-wave superconductors. This proximity-induced superconductivity is modeled by the Dirac-Bogoliubov-de Gennes Hamiltonian,

$$\mathcal{H} = \begin{pmatrix} h_+ & \hat{\Delta} \\ \hat{\Delta}^\dagger & h_- \end{pmatrix}, \tag{4.1}$$

where

$$h_\pm = -i\hbar v_F(\sigma_x\partial_x \pm \sigma_y\partial_y) \mp \mu(x), \tag{4.2}$$

$$\hat{\Delta} = i\sigma_y\Delta(x). \tag{4.3}$$

In the x-direction we have open boundary conditions and periodic boundary conditions in the y-direction, leading to plane wave ($exp(ik_yx)$) solutions, with k_y as a good quantum number. $\Delta(x)$ is the spatially dependent order parameter. $\mu(x)$ is the spatially dependent chemical potential, v_F is the Fermi velocity, and σ_i are the Pauli matrices.

$\Delta(x)$ is restricted to zero in the regions with where the superconductor is not in contact through a Heaviside step function. ϕ_i (i=1,2) are the phases of the superconductor order parameters of

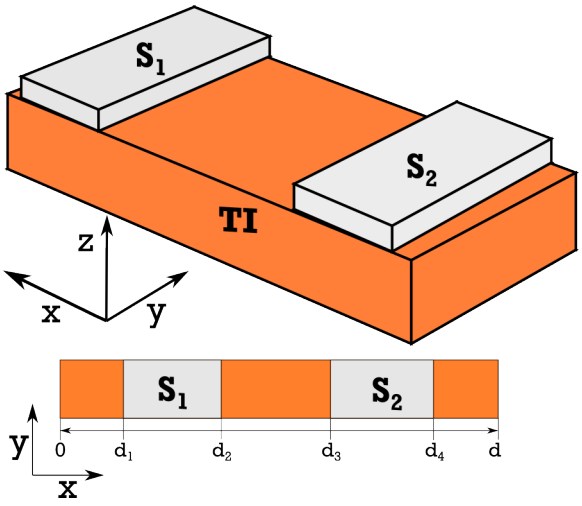

Figure 4.1: (color online) Schematic (not to scale) of superconducting Josephson junction. S_1 and S_2 are the two superconducting leads that have phases of zero and π respectively.

the two superconductor leads. In this setup we restrict the phase difference between the two superconducting ϕ to be either 0 or π, otherwise we would have to consider possible super-current flow across the surface.

The eigen wave function,

$$\psi_n = (u_{n\uparrow}, u_{n\downarrow}, v_{n\uparrow}, v_{n\downarrow})^T , \tag{4.4}$$

which satisfies $\mathcal{H}\psi_n = \epsilon_n\psi_n$, represents the BdG particle ($u_\sigma(k_y, x)$), and hole ($v_\sigma(k_y, x)$) spatial wave amplitudes with their respective spins. For berevity the energy index n will be supressed from here on.

We note the form of $h_\pm$ is derived from the TI k-space surface Hamiltonian, $H(k) = \hbar v_F \vec{\sigma}\cdot\vec{k} - \mu$, and its Time-reversed hole equivalent, $-H^*(-k) = \hbar v_F \vec{\sigma}^*\cdot\vec{k} + \mu$ by performing a substitution from k-space to real space ($k_i \rightarrow -i\partial_i$). We write the chemical potential as a spatially-dependent expression

$$\mu(x) = \begin{cases} \mathcal{E}_F, & (d_1 < x < d_2) \text{ or } (d_3 < x < d_4) \\ \mu, & \text{elsewhere} \end{cases} , \tag{4.5}$$

where $\mathcal{E}_F$ is the Fermi energy of the superconducting portion of the TI and μ is the tuned chemical potential of the metallic TI.

To self-consistently solve this system, we must start with an initial order parameter profile. We use a step function profile:

$$\Delta(x) = \begin{cases} \Delta_0, & (d_1 < x < d_2) \\ \Delta_0 e^{i\phi}, & (d_3 < x < d_4) \\ 0, & \text{elsewhere} \end{cases} \tag{4.6}$$

Once the eigen system of the BdG equation is solved, we use the wave function to calculate the order parameter in the following gap equation

$$\Delta(x) = g(x) \int dk_y \sum_n{}' u_{n\uparrow}(k_y, x) v^*_{n\downarrow}(k_y, x) \tag{4.7}$$

Where $g(x)$ is defined as a contact pairing potential spatially as:

$$g(x) = \begin{cases} g_0, & (d_1 < x < d_2) \text{ or } (d_3 < x < d_4) \\ 0, & \text{elsewhere} \end{cases} \tag{4.8}$$

After calculating a new order parameter, it is fed back into the Hamiltonian and the process is repeated until the difference between subsequent iterations of $\Delta(x)$ is under a desired small value.

In order to numerically solve this system, we employ the Fourier expansion technique by Valls et al **??** and the authors **??**. Details of this expansion are covered in said references but the general approach is as follows. We expand u, v, Δ as

$$u_\sigma(x) = \sum_{m=1}^{N} u_{m\sigma}\sqrt{2/d}\sin(k_m x) \tag{4.9}$$

$$v_\sigma(x) = \sum_{m=1}^{N} v_{m\sigma}\sqrt{2/d}\sin(k_m x) \tag{4.10}$$

$$\Delta(x) = \sum_{m=1}^{N} \Delta_m\sqrt{2/d}\sin(k_m x) \tag{4.11}$$

where $k_m = m\pi/d$. The cutoff, N, is chosen as $\hbar v_f k_m = \mathcal{E}_F + \omega_D$, where ω_d, the Debye frequency, is taken to be about $0.1\mathcal{E}_F$.This expansion results in a 4N $\times$ 4N matrix Hamiltonian of:

$$\mathcal{H} = \begin{pmatrix} -\mu_{nm} & \mathcal{K}^-_{nm} & 0 & \hat{\Delta}_{nm} \\ \mathcal{K}^+_{mn} & -\mu_{nm} & -\hat{\Delta}_{nm} & 0 \\ 0 & -\hat{\Delta}^*_{nm} & \mu_{nm} & \mathcal{K}^+_{nm} \\ \hat{\Delta}^*_{nm} & 0 & \mathcal{K}^-_{mn} & \mu_{nm} \end{pmatrix}, \tag{4.12}$$

with

$$\mathcal{K}^\pm_{nm} = -i\hbar v_F(k_m B_{nm} \pm k_y\delta_{nm}), \tag{4.13}$$

$$B_{nm} = \frac{2}{d}\int_0^d \sin(k_n x)\cos(k_m x)dx \tag{4.14}$$

$$\mu_{nm} = \frac{2}{d}\int_0^d \mu(x)\sin(k_n x)\sin(k_m x)dx \tag{4.15}$$

$$\hat{\Delta}_{nm} = \frac{2}{d}\int_0^d \Delta(x)\sin(k_n x)\sin(k_m x)dx \tag{4.16}$$

in the basis of

$$\psi = (u_{n\uparrow 1}...u_{n\uparrow N}, u_{n\downarrow 1}...u_{n\downarrow N}, v_{n\uparrow 1}...v_{n\uparrow N}, v_{n\downarrow 1}...v_{n\downarrow N},)^T,$$

Using these techniques, we will solve two different types of S-TI-S Josephson junction structures, one with a phase difference of $\phi = 0$ and one with a phase difference of $\phi = \pi$. These two structures offer very different physics.

4.3 Energy Spectrum

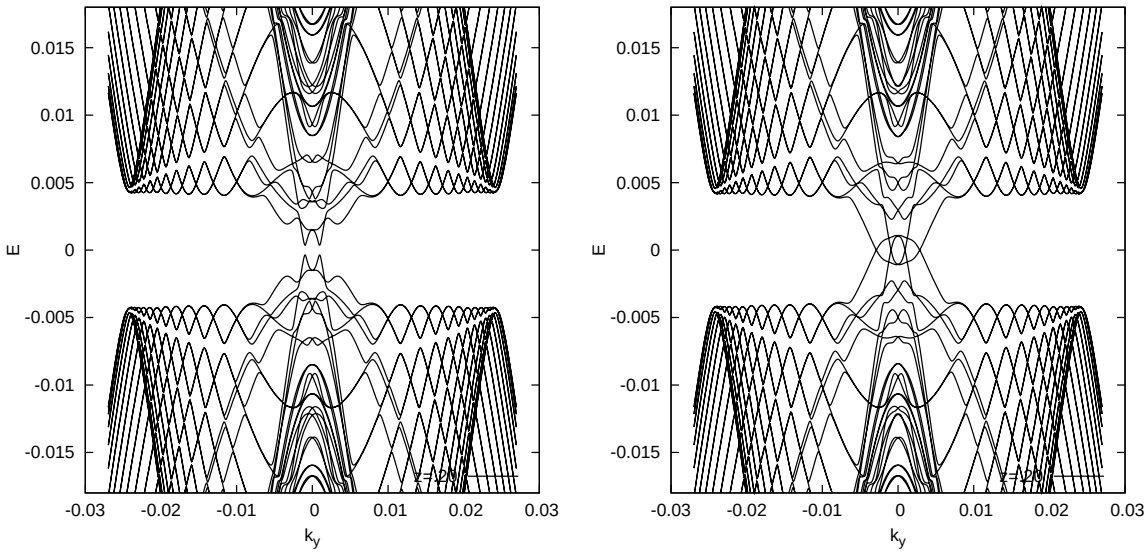

Figure 4.2: Energy spectrum of zero-bias (left) and π-bias (right) junction. The TI chemical potential is set to 5 meV. Energy is in units of eV. k_y in units of Å^{-1}

We calculate the energy spectrum as a function of of k_y for the two types of junctions, zero-biased and π-biased. It is clear from figure 4.2 that in the zero junction, the energy is fully gapped though there are subgap states that reside below the superconducting energy gap. In contrast, the π junction, is *not* gapped but rather gapless. The symmetric nature of the energies in BdG formalism allows degenerate zero-energies to exist and these zero energies are the signature for Majorana modes. All spectrum calculations from μ=0 to $\mu \approx \mathcal{E}_F$ are gapless (gapped) for the π (zero) biased junction.

These gapless modes are the signature of a Topological phase transition. Just as the bulk of a TI is gapped and the surface is gapless, the same can be said about the "bulk" of a S-TI (zero phase) which goes through a phase transition (π phase) into a Topological superconductor with gapless modes.

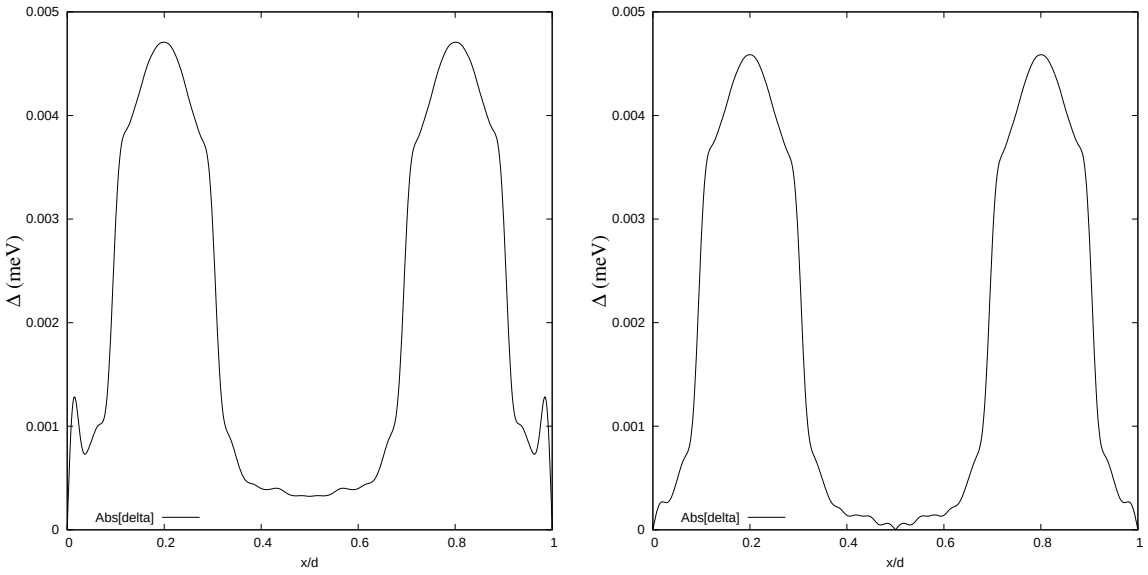

Figure 4.3: The absolute value of the singlet correlation profiles of the zero (left) and π (right) junctions. The π junction falls to zero at the midpoint. The left side of the midpoint is positive valued while the right side is negative valued. Energy of the order parameter is measured in eV and x/d is the dimension-less relative distance along the structure.

4.4 Order Parameter and Singlet Correlation

In calculating the order parameter, $\Delta(x)$, from equation 4.2 we also calculated the singlet correlation function, $F_{\uparrow\downarrow}(x)$ which is not restricted by the step function pairing potential, $g(x)$. This restriction simply sets the value of $\Delta(x)$ to zero in the non-superconducting regions of the structure. For brevity, we omit $\Delta(x)$ in favor of $F_{\uparrow\downarrow}(x)$, because it reveals better the proximity induced superconducting correlations in the non-superconducting region.

We can see that from Fig. 4.3 $F_{\uparrow\downarrow}(x)$ differs greatly between the two structures. In the π junction we see a necessary drop in the magnitude to a zero value at the halfway mark of the junction. This singularity is required in order for the phase of to switch from 0 to π from the left to the right side of the junction. A similar story occurs in the order parameter of a vortex, where the core of the vortex also has a zero value to allow the phase to change sign from one side of the center to another. The zero junction on the other hand has a very interesting "long-range" correlation. This is a by product of the spin-momentum entanglement existing on the TI, which is a fabulous host to $F_{\uparrow\downarrow}(x)$ type of correlation. This story exists in the cousin of the TI, graphene, where Valls et al found a similar constant-like value for the correlation [58].

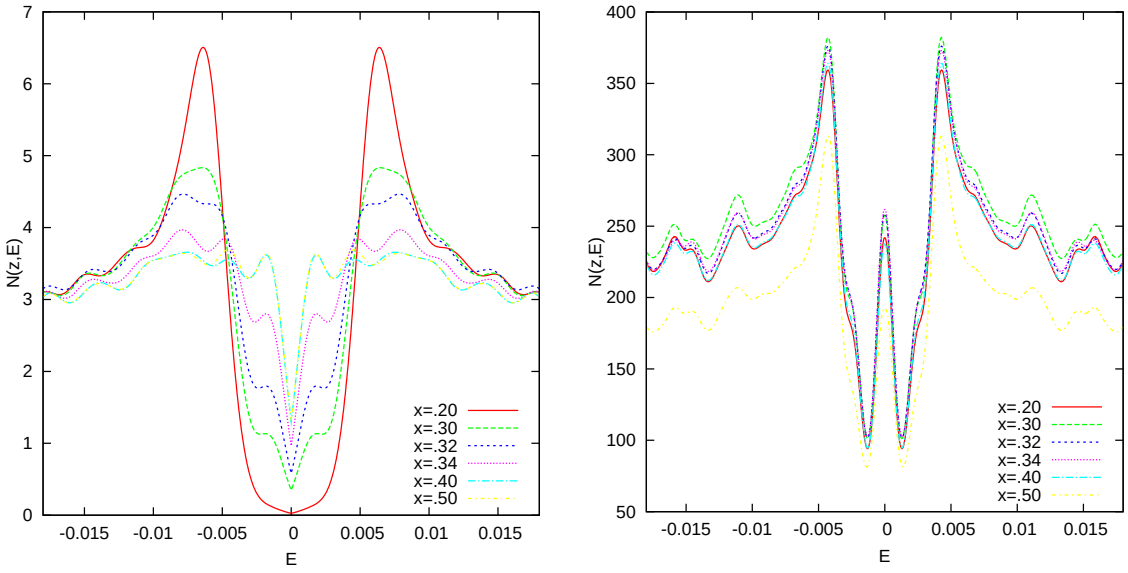

Figure 4.4: Local density of states at different positions in the heterostructure. Left (right) is the zero (π) biased junction. Energy in units of eV.

4.5 Local Density of States

Plotted in figure 4.4 are the local density of states of the two junction types with $\mu \approx \mathcal{E}_F$. Clearly both plots show very different behaviors, but interesting ones at least. On the plot of the LDOS of the zero junction we can see a second bump begin to rise essentially forming a "second gap" as it is sometimes known. This second gap is a product of the linear density of states for the TI.

We can also see from the π junction that a peak arises at the zero energy. This peak has been discussed in many literature describing experimental results. An example is posted in figure [**?**] that shows the dI/dV curve is a S-TI structure. Though differing in describing physics, they still show an interestingly similar zero-bias peak. The peak arises from the many zero energy states found especially when the TI chemical potential nears the Fermi energy ($\mu \approx \mathcal{E}_F$). It is evident from this plots that an emergence of states exist within the superconducting gap. These subgap states are a result of the "closed gap" of the π junction that shows a topological transition from the zero junction.

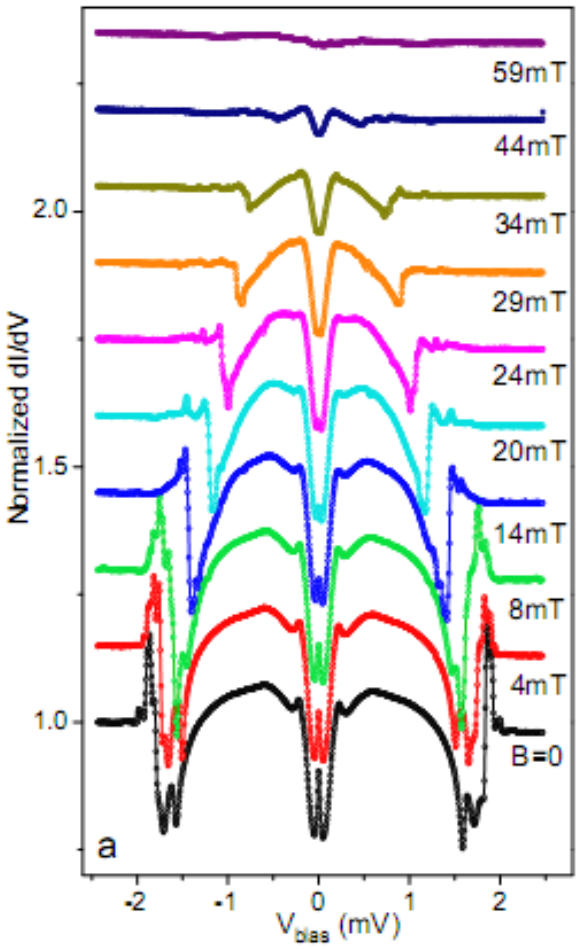

Figure 4.5: dI/dV curve of experimental results of a S-TI structure from arxiv:1105.0229 (F. Yang et al).

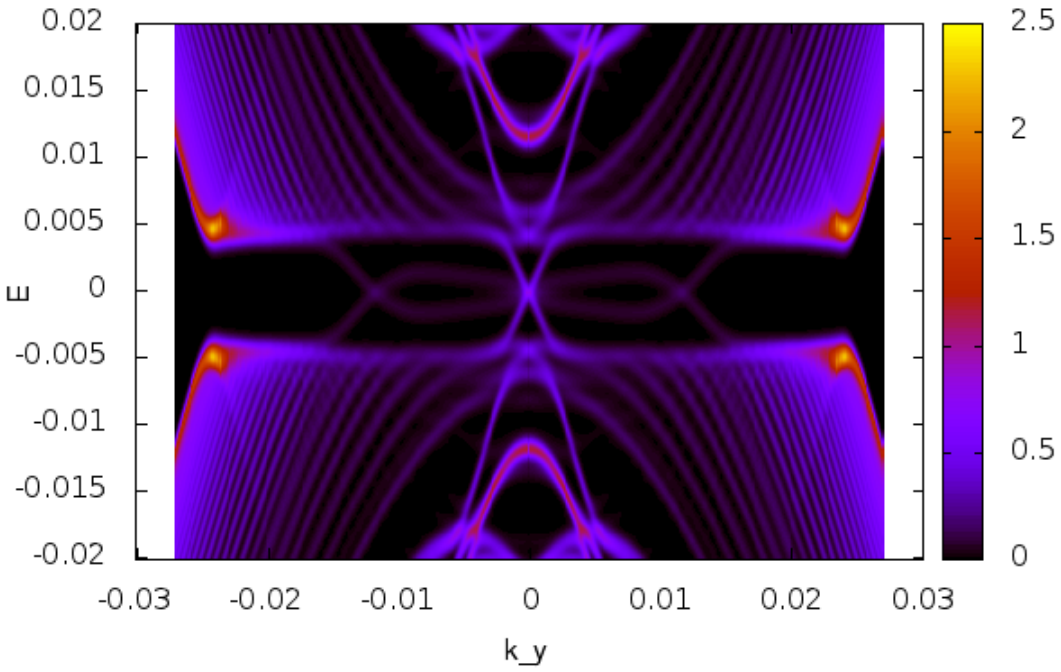

Figure 4.6: Local spectral function near the midpoint ($\approx .55$) of the π junction heterostructure. Left (right) is the zero (π) biased junction. Energy in units of eV. k_y in units of Å^{-1}

4.6 Spectral Function

Lastly, we show the local spectral function of the π junction structure. The zero junction does not illuminate any interesting results for this proposal at the moment. Though the energy spectrum gave a very nice detailed description of the energy levels of the whole system, the spectral function shows the local density of the states. We can see the gapless modes including the possible Majorana modes located at zero energy for three values of k_y. A detailed understanding of the spectral function of the π junction is the subject of future work.

4.7 Summary

Much of the physics has been calculated and plotted in this structure. What simply remains is to write up all the results and submit them to Physical Review. Other calculations could be developed from these results. Calculating the Ginzburg-Landau free energy would give us insight on whether the zero or π junction would be the natural stable setup. Additionally a Josephson junction on the 3D bulk can also be done to determine more physics of this type.

Chapter 5

TI-FET: MOSFET with a Topological Insulator

5.1 Introduction

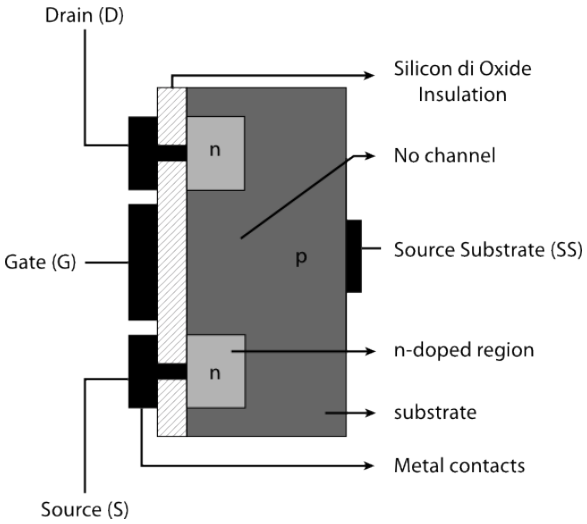

Figure 5.1: (left) A proposed heterostructure that exploits the exotic surface states that differ from the bulk in a TI. (right) A typical n-type MOSFET.

In this chapter I present ideas originally proposed by Professor Qialang Li of the Electrical and Computer Engineering department. Professor Li has suggested to utilize a TI in a MOSFET type of structure as a floating gate. In addition the Xue group has proposed [need cite] to use a TI as a current channel to make a new generation of FETs. To give an overview of such ideas, I first present a quick introduction on how a MOSFET works, then I outline these two proposals. Lastly, I will describe the general outline of how to simulate the physics of these structures to give insight in designing them.

5.2 MOSFET

The Metal Oxide Silicon Field Effect Transistor (MOSFET) is the standard component in digital electronics. It is used to store and read information when a voltage is stored on the Metal gate (G) in a capacitive form. It is used in intricate, clever methods to process binary logic. The impact of the MOSFET on society is grossly understated in this section, but the main point I try to impress upon is it's ability to digitize the world's information in robust precision.

As seen in the Figure 5.1, a MOSFET is composed of a voltage biasing gate (G); a pair of n-doped silicon leads, the drain (D) and the source (S); a channel composed of a p-doped silicon. The simple operation scheme is the following. When a voltage, ($\approx$ 5V) is applied across G to the bottom of the channel, the electrons sitting on the gate induce a drop in the chemical potential in the channel. This drop allows a current to develop when the Source and Drain are biased, where otherwise no current would flow across the n-p-n region when no voltage is applied across the gate. This is known as the transistor effect, hence, the moniker field effect transistor (FET).

When the Drain to Source voltage, V_{DS}, is varied, the current saturates after a certain threshold as seen in figure 5.2. This single valued saturation is critical for reading out the Gate Voltage, V_G.

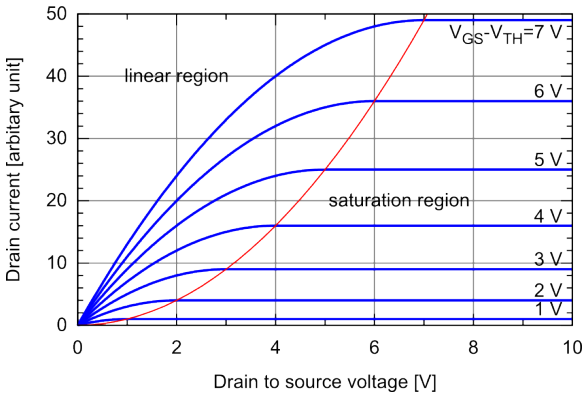

Figure 5.2: A typical MOSFET IV relation plot for various values of V_{GS}.

5.3 TI as the Floating Gate

Professor Qilian Li suggested to use a TI as a programmable voltage gate in a floating gate MOSFET. The reasoning follows as such. A TI has surface states that differ from the bulk states. Together, these states should combine for an unconventional density of states. This unconventional nature should allow an unconventional storage mechanism as well. This could allow for a new device of non-volatile information storage.

In order to achieve this, a simulation needs to be performed. This simulation will be, ideally, done as follows. A lattice tight-binding calculation of a 3D TI, such as Bi_2Te_3, will be used to calculated the energy spectrum. One of the input parameters would be the "programming voltage" which in essence controls the chemical potential. Based on the energy spectrum, we calculate the local density of states using the formula

$$N_{l\sigma}(\omega > 0) = \int dz d\mathbf{k}_{\parallel} \sum_{n} |\psi_{n,l\sigma}(\mathbf{k}_{\parallel}, z)|^2 \delta(\omega - \epsilon_n). \tag{5.1}$$

Using the DOS, we can further calculate the stored charge onto the TI as a function of voltage. This voltage relation forms a basis to investigate the DC and AC characteristics of the whole device.

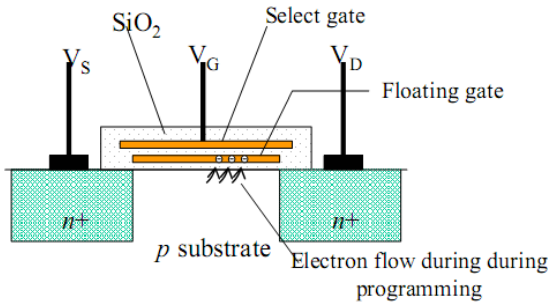

Figure 5.3: A floating gate MOSFET. The main difference seen here is the additional "programming gate" above the voltage gate normally seen in a MOSFET.

5.4 TI as the Current Channel

Though this proposal was already presented in Nature Nanotechnology by Qi-Kun Xue, no theoretical nor experimental work has been presented. This means the game is open for anyone to demonstrate the TI-FET in the near future.

As described above, the MOSFET uses a p type channel to be controlled by the gate voltage. This voltage determines whether a current will pass from one n doped region (Source) to the other n doped region (Drain). But rather than using a p type region to allow current to pass, a possibility is to use a TI because the TI surface is metallic. These metallic states essentially can act like semiconductors because they also could potentially have their current characteristics manipulated by the gate voltage.

The method in simulating this device is as follows. A dI/dV conductance calculation would be done for a Metal-TI-Metal setup on a finite sized lattice. To calculate the conductance we would need to find the Green's function response of the system to find the scattering matrix. Once the S-matrix is found, using Landauer formalism, we can calculate the conductance through a simple relation.

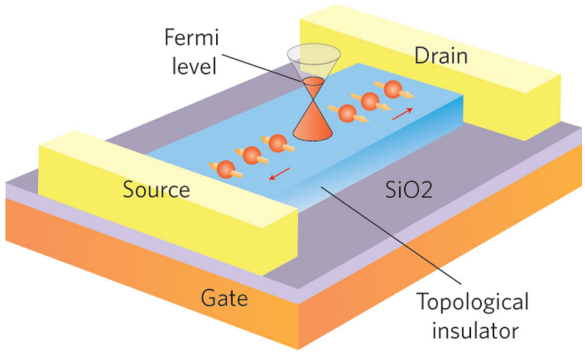

Figure 5.4: (left) A proposed heterostructure that exploits the exotic surface states that differ from the bulk in a TI. (right) A typical n-type MOSFET.

5.5 Summary

These calculations are not trivial but computationally tractable. The results would be very illuminating. They would guide future experiments in realizing a TI-FET structure.

Bibliography

[1] J. Alicea, Physical Review B **81**, 125318 (2010).

[2] T. Yokoyama, Y. Tanaka, and N. Nagaosa, Phys. Rev. Lett. **102**, 166801 (2009).

[3] V. Heine, Phys. Rev. **138**, A1689 (1965).

[4] S. G. Louie and M. L. Cohen, Phys. Rev. B **13**, 2461 (1976).

[5] J. Tersoff, Phys. Rev. Lett. **52**, 465 (1984).

[6] L. Fu, C. L. Kane, and E. J. Mele, Phys. Rev. Lett. **98**, 106803 (2007).

[7] J. E. Moore and L. Balents, Phys. Rev. B **75**, 121306 (2007).

[8] R. Roy, Phys. Rev. B **79**, 195322 (2009).

[9] D. Hsieh et al., Nature **452**, 970 (2008).

[10] Y. Xia et al., Nat Phys **5**, 398 (2009).

[11] H. Zhang et al., Nat Phys **5**, 438 (2009).

[12] Y. L. Chen et al., Science **325**, 178 (2009).

[13] D. Hsieh et al., Nature **460**, 1101 (2009).

[14] A. A. Burkov and D. G. Hawthorn, Phys. Rev. Lett. **105**, 066802 (2010).

[15] X.-L. Qi and S.-C. Zhang, Physics Today **63**, 33 (2010).

[16] M. Z. Hasan and C. L. Kane, ArXiv:1002.3895 (2010).

[17] X. Qi and S. Zhang, ArXiv:1008.2026 (2010).

[18] A. Millis, D. Rainer, and J. A. Sauls, Phys. Rev. B **38**, 4504 (1988).

[19] T. D. Stanescu, J. D. Sau, R. M. Lutchyn, and S. Das Sarma, Phys. Rev. B **81**, 241310 (2010).

[20] L. Fu and C. L. Kane, Phys. Rev. Lett. **100**, 096407 (2008).

[21] J. G. Checkelsky, Y. S. Hor, R. J. Cava, and N. P. Ong, ArXiv:1003.3883 (2010).

[22] I. V. Tokatly, A. G. Tsibizov, and A. A. Gorbatsevich, Phys. Rev. B **65**, 165328 (2002).

[23] D. J. BenDaniel and C. B. Duke, Phys. Rev. **152**, 683 (1966).

[24] W. Kohn, Phys. Rev. **115**, 809 (1959).

[25] E. I. Blount, *Solid State Physics*, volume 13, Academic Press, 1962.

[26] V. Heine, Proceedings of the Physical Society (London) **81**, 300 (1963).

[27] Y.-C. Chang and J. N. Schulman, Phys. Rev. B **25**, 3975 (1982).

[28] X.-L. Qi, T. L. Hughes, and S.-C. Zhang, Phys. Rev. B **78**, 195424 (2008).

[29] N. F. Mott and H. S. Massey, *The Theory of Atomic Collisions*, Oxford University Press, 3rd edition, 1965.

[30] F. Garcia-Moliner and V. R. Velasco, *Theory of single and multiple interfaces*, World Scientific, 1992.

[31] L. Fu and C. L. Kane, Physical Review Letters **100**, 096407 (2008).

[32] N. Read and D. Green, Physical Review B **61**, 10267 (2000).

[33] X. Qi and S. Zhang, Reviews of Modern Physics **83**, 1057 (2011).

[34] R. M. Lutchyn, J. D. Sau, and S. Das Sarma, Physical Review Letters **105**, 077001 (2010).

[35] J. D. Sau, S. Tewari, R. M. Lutchyn, T. D. Stanescu, and S. Das Sarma, Physical Review B **82**, 214509 (2010).

[36] L. Mao and C. Zhang, Physical Review B **82**, 174506 (2010).

[37] L. Mao, J. Shi, Q. Niu, and C. Zhang, Physical Review Letters **106**, 157003 (2011).

[38] Y. Tanaka, T. Yokoyama, and N. Nagaosa, Physical Review Letters **103**, 107002 (2009).

[39] J. Linder, Y. Tanaka, T. Yokoyama, A. Sudb, and N. Nagaosa, Physical Review B **81**, 184525 (2010).

[40] J. Linder, Y. Tanaka, T. Yokoyama, A. Sudb, and N. Nagaosa, Physical Review Letters **104**, 067001 (2010).

[41] B. Sacp et al., Nat Commun **2**, 575 (2011).

[42] M. Veldhorst et al., Bulletin of the American Physical Society **Volume 56, Number 1**.

[43] D. M. Zhang et al., Bulletin of the American Physical Society **Volume 56, Number 1**.

[44] A. M. Black-Schaffer, Physical Review B **83**, 060504 (2011).

[45] Y. S. Hor et al., Physical Review Letters **104**, 057001 (2010).

[46] L. A. Wray et al., Nat Phys **6**, 855 (2010).

[47] M. Kriener, K. Segawa, Z. Ren, S. Sasaki, and Y. Ando, Physical Review Letters **106**, 127004 (2011).

[48] H. Zhang et al., Nat Phys **5**, 438 (2009).

[49] W. Zhang, R. Yu, H. Zhang, X. Dai, and Z. Fang, New Journal of Physics **12**, 065013 (2010).

[50] E. Zhao, C. Zhang, and M. Lababidi, ArXiv:1005.3064 (2010).

[51] K. Halterman and O. T. Valls, Physical Review B **65**, 014509 (2001).

[52] B. P. Stojkovi and O. T. Valls, Physical Review B **47**, 5922 (1993).

[53] T. Tokuyasu, J. A. Sauls, and D. Rainer, Phys. Rev. B **38**, 8823 (1988).

[54] M. Eschrig, Phys. Rev. B **80**, 134511 (2009).

[55] Y. Tanaka, T. Yokoyama, and N. Nagaosa, Phys. Rev. Lett. **103**, 107002 (2009).

[56] F. S. Bergeret, A. F. Volkov, and K. B. Efetov, Reviews of Modern Physics **77**, 1321 (2005).

[57] J. B.D., Physics Letters **1**, 251 (1962).

[58] K. Halterman, O. T. Valls, and M. Alidoust, Physical Review B **84**, 064509 (2011).